Experimental investigation of the radiation produced by the passage of 10-GeV electrons and positrons through single crystals

É. N. Tsyganov

Joint Institute for Nuclear Research, Dubna

Fiz. Elem. Chastits At. Yadra **20**, 5–50 (January–February 1989)

A facility for investigating the radiation produced by high-energy electrons and positrons is described. The facility Kristall was built at the Institute of High Energy Physics in 1980. It ensured a resolution in the angle of entry of the particles into a crystal of about 6 μrad, and in the angle of exit of 30 μrad; for some events the emission angles of the γ rays were measured with an accuracy of about 4 μrad. The targets were dislocation-free single crystals. Experiments made with Kristall gave information about the radiation produced in the case of axial and planar channeling of 10-GeV electrons and positrons in silicon and germanium single crystals. The properties of the electromagnetic radiation for different angles of entry into the crystal and also data on the radiative energy losses are given. Angular distributions of the radiation were measured for the first time. Data are also given on the coherent bremsstrahlung of relativistic electrons and positrons in thin silicon single crystals.

INTRODUCTION

Intense sources of photons from the ultraviolet to the hard x-ray range have many practical applications. Important examples of radiation are Cherenkov radiation, radiation in artificial periodic structures, bremsstrahlung, etc.

The radiation that arises when light particles are channeled in single crystals is particularly interesting. The existence and characteristic properties of this radiation, for example, high spectral density and sharp directionality, were predicted theoretically by Kumakhov in 1976.[1] When our experiment was being prepared, the radiation had not yet been discovered, but in 1979 it was observed for the first time at SLAC.[2]

There have been many experimental and theoretical studies of the channeling effect. The first experimental studies of channeling were made at comparatively low energies, of the order of a few mega-electron-volts. Since then many experimental and theoretical studies have been made of channeling at high energies. In accordance with Lindhard's predictions, it has been found that the use of classical mechanics to describe channeling becomes more and more accurate with increasing energy. If the electrons have energies 1–10 GeV, the classical description of their motion is sufficiently accurate.

The main conclusions of the modern theory are as follows. Light charged particles move for a relatively long time along the channels formed by crystal planes or axes. At the same time there are spontaneous radiative transitions between levels of the transverse energy, and relativistic effects play a dual role. The relativistic growth in the mass of the particles leads to a decrease of the difference between neighboring levels of the transverse energy, i.e., of the frequency of the transverse vibrations, whereas the Doppler effect has the consequence that the energy of a radiated photon is significantly greater than the energy of the transitions between the levels of the transverse energy and also leads to a concentration of the radiation intensity in the direction of the longitudinal motion.

The intensity of this radiation is maximal under the condition of channeling.

As we noted above, the first experimental investigations in this field at high energies were made at SLAC; experiments were then performed at Tomsk and Erevan. The intensity of the radiation in the SLAC experiments was found to be significantly lower than the theoretically predicted intensity. The experiments at Tomsk and Erevan, made in 1979, indicated a high intensity of the radiation in the potentials of the crystallographic axes and planes, but they did not have sufficient accuracy.

A novelty of our work was that an experiment was performed for the first time using the modern electronic techniques of high-energy physics. This made it possible to investigate in detail for the first time the spectral characteristics of the radiation for different ranges of angles of entry of the electrons and positrons into the crystal within the critical angle of channeling. The angular distributions of the emitted photons were investigated for the first time. The properties of the radiation produced in the case of planar channeling of ultrarelativistic electrons were studied in detail for the first time.

The results of our investigations were published in Refs. 3–22.

1. THE EXPERIMENT

The facility Kristall was built in 1980 at the Institute of High Energy Physics to investigate the properties of the radiation produced by the channeling of high-energy electrons and positrons. The basis of its construction was an apparatus by means of which the deflection of particles by bent single crystals could be investigated. The apparatus was significantly modified and extended.

The Kristall facility is shown in Fig. 1. A beam of electrons (or positrons) was incident on a single-crystal target placed in a remote-controlled goniometer. The path of the particles before and after the target were determined by a system of drift chambers grouped into three blocks. A fourth block of drift chambers was used to determine the particle paths after the analyzing magnet. The photons emitted in the target were detected by means of a CsI(Tl) scintillation crystal surrounded by a lead shield and a system of anticoincidence counters. The photon emission angles were measured by means of a block of drift chambers with an aligned converter placed directly in front of the radiator of the photon spectrometer. The secondary electrons (positrons) were

 0090-4759/89/010001-21$04.40

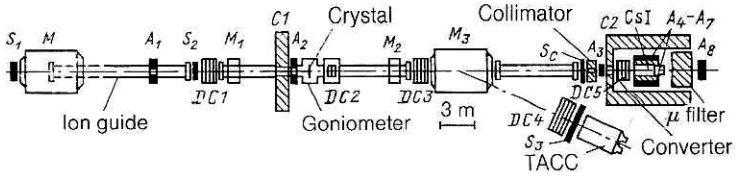

FIG. 1. Arrangement of the experiment: $S_1, S_2 S_3, A_1-A_8$ are scintillation counters; DC 1-DC 5 are blocks of drift-chambers; TACC is a total absorption Cherenkov counter with lead-glass radiator; CsI(Tl) is a photon spectrometer based on a cesium–iodine single crystal; C 1 and C 2 are collimators; M, M_1, M_2, and M_3 are bending magnets.

identified by means of lead-glass shower Cherenkov counters, which covered the range of momenta from 5 to 10 GeV/c. The equipment was triggered by a system of coincidence and anticoincidence counters and was operated online to an EC-1040 computer.

Investigations were made with beams of electrons and positrons. The source of the electrons and positrons was a converter outside the magnetic field of the accelerator at a direction with angle of about 2.5° relative to the primary proton beam. The electrons (positrons) formed in the converter were deflected into the channel by means of a pulsed magnet. The admixture of hadrons in the electron and positron beams did not exceed 1%. The beams had very similar characteristics, and the transition from the one type of particle to the other did not require much time. The beam intensity at energy 10 GeV was about 10^5 particles per accelerator cycle; the number of protons incident on the target was about 10^{12}. The momentum separation of the beams had an rms spread of about 130 MeV/c. In the region of the crystal the beam had an rms angular divergence of about $\pm$ 1 mrad, and its diameter was about 20 mm (FWHM). The beam parameters were adjusted and controlled by means of the experimental Kristall facility. The reconstruction of the particle paths by means of the drift chambers made it possible to obtain the profile of the beam and its angular characteristics.

The energies of the radiation produced in the single crystals were investigated by a CsI(Tl) photon spectrometer. In order to obtain by means of it true energy spectra it was necessary to have only single radiation events, i.e., the probability of photon emission from the target had to be much less than unity. For this, it was necessary to use crystal samples with a thickness of not more than 100 μm.

As the particles pass through the equipment, not only the investigated radiation but also background bremsstrahlung in the matter of the experimental equipment (scintillation counters, mylar windows of the ion guide, modules of the drift chambers, etc.) arises. The intensity of the bremsstrahlung from a silicon single crystal of thickness 100 μm oriented randomly was not more than 2% of the intensity of the background radiation in the matter of the equipment. Clearly, the optimization of the background conditions in the experiment was a serious problem, and reduction in the amount of matter was the first step in its solution. The matter of the scintillation counters and the mylar windows of the ion guide was minimized. The entire beam tract in the facility, the total length of which was about 70 m, was evacuated, except for the scintillation counter S_2, the modules of the drift chambers, and the secondary-particle spectrometer. The drift chamber DC 2 was operated at a reduced pressure, and all its wires were taken outside the working region. The total amount of matter in the facility after the minimization was about 5×10^{-2} radiation lengths. To ensure that the background radiation in the counter S_1 and the entrance window of the ion guide did not enter the opening of the photon spectrometer, the counter was placed in front of the distributing magnet M, and the ion guide began in the middle of this magnet. Background measurements showed that the main contribution to the remaining background was made by the radiation in the counter S_2 and in the modules of the drift chambers DC 1 and DC 3. Clearing magnets were used to decrease the background further. Since the photons are emitted in a narrow angular range relative to the charged particle, magnets can be used to separate spatially the radiation produced before and after the crystal. The use of the magnet M_1 after the first block of chambers with deflection angle 3 mrad and the magnet M_2 in front of the third block of chambers with deflection angle 5 mrad made it possible to reduce the background sharply. Then only about 1% of the background due to the matter of the facility entered the opening of the photon spectrometer, and this was perfectly satisfactory.

Drift chambers arranged in five blocks were used as coordinate detectors. The chambers DC 1, DC 3, and DC 4 contained four X and four Y planes each. The drift planes in the DC 1 and DC 3 blocks measured 12.5×12.5 cm, and in the block DC 4 they measured 25×25 cm. Signal wires of diameter 20 μm made from gilded tungsten were wound with pitch 42 mm in such a way that the maximal length of the drift gap was 21 mm. The working gas was a mixture of 67.2% argon + 30.3% isobutane + 2.5% methyl vapor. The signals from the wires were sent to an amplifying discriminator, which had a response threshold of about 2 μA. The chambers were placed together with the amplifiers in screening thermally stabilized boxes.

The low-pressure drift chamber DC 2, which consisted of two X and two Y planes, was specially developed for the experiment. The use of a standard block of drift chambers at the position of DC 2 was undesirable because of the high multiple scattering, of order 100 μrad. For comparison, we note that the critical angle for channeling of positively charged particles at energy 10 GeV for a (110) plane is about 65 μrad. In addition, as noted above, it was necessary to minimize the background produced in the matter of this detector.

The matter in the chamber DC 2 was reduced by minimizing the thickness of the mylar windows, removing all the wires from the working region, and reducing the gas pressure. The chamber was placed immediately after the goniometer and was mounted in the ion guide of the facility. Its gas space was bounded by mylar windows of thickness 12 μm. The construction of the chamber eliminated left–right ambiguity in the determination of the coordinates. Spurious tracks could be eliminated on the basis of the sum of the times of drift from two planes. Each plane of the chamber was divided into two drift gaps of extension 5 mm, and the signals from two wires of one plane were added. The working region of the chamber measured 10×10 mm. The chamber was constructed from frames of glass-reinforced epoxy with an inner window of 80×80 mm. The gas mixture consisted

of 62% argon, 28% isobutane, and 10% methyl vapor. The pressure of the working gas in the experiment was 250 mm Hg, and the amount of matter in the chamber along the beam was about 5×10^{-4} radiation lengths. The signals from the chamber were detected by means of an amplifying discriminator having a threshold of about 0.5 μA and placed in a screening box.

The drift chambers *DC* 1, *DC* 2, and *DC* 3 were used to determine the paths of the electrons (or positrons) before and after the target. The total error of the block of ordinary chambers (of four planes) was about 50 μm, and the error of the block of low-pressure drift chambers (of two planes) was about 90 μm. This ensured a resolution with respect to the angle of entry of about 6 μrad in projection, and with respect to the angle of exit with allowance for multiple scattering in the chamber *DC* 2 of about 30 μrad. Estimates showed that the resolution of the facility with respect to the scattering angle in one projection must have been about 35 μrad. The rms deviation of the scattering angles in a run without the target was 33 μrad, and this corresponds to the estimates.

The fourth block of drift chambers, *DC* 4, was used to measure the momentum of the secondary particles with an error less than $\pm$ 1%, this error being determined by the uniformity of the field of the analyzing magnet and the accuracy of the magnetic measurements.

The fifth block of drift chambers, *DC* 5, with a built-in converter was used to measure the angles of emission of the photons from the crystal on the basis of the reconstructed coordinate of the vertex of the resulting electron–positron pair.

The block *DC* 5 consisted of three drift planes analogous to the planes in *DC* 1 and *DC* 3; in the three planes, two, three, and four signal wires, respectively, were activated. To minimize the error in the reconstruction of the point of conversion of the photon, the converter was placed as close as possible to the cathode plane of the first drift gap. The converter was made sufficiently thin to avoid a deterioration of the energy resolution of the photon spectrometer and to prevent the development of an electromagnetic shower, which would increase the coordinate error of the instrument. A copper converter with a thickness of 0.064 radiation lengths was used.

In conjunction with the chambers *DC* 2 and *DC* 3 the instrument ensured measurement of the angles of the photons in the Y projection with an error of about 4 μrad.

The signal from the scintillation counter S_2, shaped by the amplifying discriminator, was sent along a high-frequency cable to the hall of the experimentalists, where it was regenerated. The cable ensured a delay of about 400 nsec, which was needed to shape the "Start TDC" signal. The signals from the drift wires reached the "Stop" input of the time-to-digital converters, which had a scale value of 300 psec. In the chambers *DC* 1–*DC* 4 each signal wire had its own TDC channel. In the drift-chamber block *DC* 5, where it was necessary to ensure readout of two signals from each wire in order to detect the electron–positron pairs, a special block that separated each secondary pulse was added to the tract. Thus, for each of the wires there were two TDC channels. The channels of the detecting electronics and the TDC calibration were checked by means of "Test" signals, which were sent to the amplifier inputs immediately after the accelerator pulse. For the TDC calibration, the "Test" signals were delayed relative to the "Start" pulse. Different delays were specified by means of a quartz oscillator and were chosen to cover the working range of the converters.

Dislocation-free silicon single crystals (the number of dislocations did not exceed 10 cm^{-2}) were used as targets. The crystals were cut at right angles to the investigated crystallographic axes with an accuracy of about 0.2° and were made in the form of disks of thickness 0.5 mm and more. To obtain thin targets, the central part of the sample, with diameter 18 mm, was etched down to the necessary size. The minimal target thickness was about 20 μm, and the thickest of the samples had a thickness of 10 mm. The single crystals were held in a clamp that made it possible to position up to four different samples simultaneously. The clamp was placed in the goniometer and was remote-controlled. Each of the samples was inserted in a reference ring made in the form of a semiconductor detector, the signals from which were used when the facility was triggered in order to center the crystals by means of the paths of the beam particles. In the preliminary adjustment, the flat surface of each crystal was aligned at right angles to the beam axis by means of a reflected laser beam. Rotation of the crystal in the goniometer made it possible to determine the orientation dependence of the number of photons on the angle of rotation of the crystal. The crystallographic axes and planes were identified and their positions determined by means of the peaks in this dependence. The goniometric system made it possible to rotate the crystal by remote control around two mutually perpendicular axes in steps of 0.001°.

One of the main aims of the experiment was to investigate the energy spectra of the photons produced in a crystal by the passage of high-energy electrons and positrons. At energy 10 GeV of the primary particles, the peaks of these spectra for planar channeling must lie in the region up to 200 MeV and for axial channeling up to 1 GeV. For photon spectrometry in this energy range the most rational choice is a shower detector based on a scintillating radiator.

A detector was made using a CsI(Tl) single crystal in the shape of a cylinder of diameter 150 mm and length along the beam of 230 mm. The matter density of the single crystal was $\rho = 4.51$ g/cm^3, the radiation length was $X_0 = 1.8$ cm, and the radiator was scanned by a single FÉU-49 photomultiplier with a photocathode of diameter 150 mm.

The spectrometer was designed for operation in a wide dynamical range. To obtain good resolution in the region of low energies, complete collection of the photoelectrons in the photomultiplier was needed. Under these conditions the current through the photomultiplier in the real experiment in the ordinary photomultiplier regime was so high that there was a strong instability of the photomultiplier gain, the instability depending on the load on the detector. The problem was solved by reducing the gain of the photomultiplier with simultaneous increase in the amplification of the spectrometric electronics. To maintain efficient collection of photoelectrons, recommended voltages were applied to the primary electrodes of the photomultiplier. The total voltage on the divider of the photomultiplier did not exceed 660 V. In this way a good stability of the photomultiplier gain under conditions of a high load was achieved.

Tracts of detection of the signals from the photomultiplier were used to achieve the resolution of the analog-to-digital conversion in the region of low energies of the pho-

tons (about 0.1 MeV/count). The tract in which the signal was taken from the photomultiplier anode ensured measurement of energies up to about 1 GeV. The dynode tract, in which the signal was taken from the last photomultiplier dynode, had a working range up to 10 GeV. The total range of the first analog-to-digital converter of the anode tract corresponded to an energy of 200 MeV, and therefore for the detection of photons with energy 1 GeV the signal was divided further in the ratio 1:5 and passed to a secondary analog-to-digital converter. Thus, photon detection was done simultaneously in three ranges: 10–200, 10–1000, and 10–10 000 MeV with steps of 0.1, 0.5, and 5 MeV, respectively. To reduce the spread of the signals due to the drift of the "zero" a measurement of the "zero" potential of the spectrometric anode tract was made 4 μsec before the working signal.

Besides the tract for detection of the spectrometric signals a so-called time tract was organized in the system of information readout from the photon spectrometer. In it the signal from the fast output of the anode preamplifier was converted to a logic pulse. This pulse determined the time of passage of the particle through the photon spectrometer. The time was detected by means of a special time-to-digital converter with step 20 nsec in the range $\pm$ 5 μsec relative to the facility triggering signal. The time resolution of the tract was not worse than 40 nsec. The use of this information in the subsequent analysis of the data made it possible to reduce the background of random events by about 100 times.

The photon spectrometer, surrounded on four sides by the scintillation counters A_1–A_4, was placed directly after the block of the drift chambers with a built-in converter *DC* 5, in front of which there was a lead collimator with opening 80 $\times$ 80 mm. The surrounding counters were used to reject events in which a background charged particle passed through the radiator of the spectrometer. Signals from them, stored in the input register LATCH, could if necessary be connected in anticoincidence to the main signal triggering the facility. The radiator of the spectrometer was placed in a lead "shirt" that had walls of thickness 60 mm and absorbed shower particles that emerged from the radiator. The photon spectrometer and the drift chamber with the converter were surrounded by a lead shield with walls of thickness about 250 mm. The photon spectrometer was adjusted in the horizontal and vertical planes on the basis of the position of the bremsstrahlung beam from the target, which was determined by means of a scanning photon counter of sandwich type.

The spectrometer was calibrated by means of radioactive sources, and also by means of the correlation of the pulse of secondary particles and the counts of the photon spectrometer (tagged-photon method).

To correct long-period instabilities of the spectrometric tract during the accumulation of statistics, information on the ionization losses of the background μ mesons in the radiator of the spectrometer (about 130 MeV) was continuously recorded. For this every sixteenth triggering of the facility was made with the counters A_6 and A_8 connected in coincidence. The soft component of the μ mesons ($E \leqslant 1$ GeV) was eliminated by means of an absorbing filter. To correct the instabilities of the tract during a pulse of the accelerator—they usually did not exceed 3%—triggers from a light-emitting diode were used.

The resolution of the photon spectrometer at energy 1 MeV was determined by calibration using a radioactive ^{60}Co source with high photomultiplier gain and was 8% (FWHM). Under the working conditions with a potential of 660 V on the photomultiplier, tract noise of about 0.1 MeV was added. Estimates showed that at energy 100 MeV the detector had a resolution not worse than 3%.

Six types of trigger were used during the accumulation of statistics. Each trigger had its own identifier recorded in a cell of LATCH. The succession of the triggers was determined by a special block.

The main type of trigger was designed to detect events in which a primary particle radiated a photon with energy above the threshold value. Signal detection occurred when there was a signal from the beam telescope $S_1S_2A_1A_2$.

An electronic synchronization system, the control of the set of data and their detection, and also the system of communication with the computer were set up in the CAMAC standard and placed in three crates organized into a CAMAC branch by a universal branch driver. The detecting apparatus of the facility consisted of commercially available CAMAC blocks, the sequence of which determined the format of the array of physical information.

A remote computer of the type EC-1040 was used to control the facility and collect and analyze the data. The work of the program could be controlled from the hall of the experimentalists by means of the terminal DZM-180-KSR and the control panel. The results of the analysis were fed to the alphanumeric printer of the computer, and also to the display and terminal of the facility.

The facility, created to study spontaneous radiation by high-energy charged particles in single crystals, was adequate for the task. The radiation background corresponded to an amount of matter of around 5×10^{-4} radiation lengths. The facility ensured a resolution with respect to the angle of entry of the particles into the crystal of about 6 μrad and with respect to the angle of exit of about 30 μrad, while the resolution of the facility with respect to the scattering angle was about 33 μrad. The emission angles of the photons were measured for about 4% of the events, and the accuracy of the measurement was about 4 μrad.

2. INVESTIGATION OF POSITRON RADIATION IN THE CASE OF PLANAR CHANNELING

For analysis of the data, events in which a photon with energy above 5 MeV was detected were selected. It was required that the continuation of the entry track of the particle enter the opening (80 $\times$ 80 mm) of the collimator of the photon spectrometer. The signal in the total-absorption Cherenkov counter had to match in amplitude the signal from a positron with the momentum determined by means of the chamber *DC* 4 and magnet M_3. The sum of the energies of the photon and the secondary positron had to be equal to the energy of the primary positron.

A silicon crystal of thickness 113 μm was oriented with the plane (110) parallel to the beam direction. The angle between the beam and the ⟨111⟩ axis of the crystal was 0.5°.

Orientation dependences

Figures 2 and 3 show the dependences of the number of emitted photons on the angle of entry of the positrons into the crystal. As in all the remaining figures, they are normalized to one incident positron. The chain line illustrates the

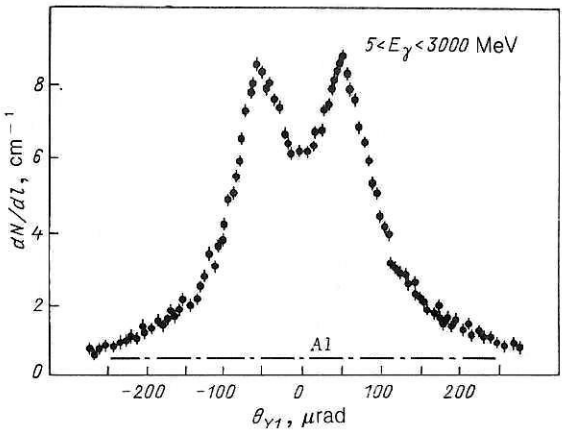

FIG. 2. Dependence of the number of radiated photons on the angle of entry of the positrons into the crystal.

analogous data obtained from an amorphous aluminum target. The critical angle for channeling of 10-GeV positrons by the (110) plane of silicon is about 65 μrad. The maximum of the probability of radiation (Fig. 2) is at positron entry angle of about 50 μrad relative to the crystallographic plane. Converted to a crystal of thickness 1 cm, about eight photons are emitted at the maximum. The displacement of the maximum of the radiation probability relative to zero angle is due to particles that radiate photons with energy above 5 MeV. This is illustrated by Fig. 3, in which events with photons in different energy ranges were selected. Figure 3 corresponds mainly to channeled (a, b) and above-barrier (c–f) particles. It can also be seen from Fig. 3 that with increasing energy of the photons the maximum of the radiation probability is shifted to larger angles (d–f).

Note that the radiation probability for particles that enter the crystal at zero angle is slightly suppressed compared with the maximal value for photons of any energy. The probability of emission of photons with energy above 360 MeV for particles that enter the crystal at angles near zero does not exceed the probability of radiation in the amorphous target (Fig. 3f).

Radiation spectra of channeled positrons

Figures 4 and 5 show the dependences of the spectral density of the radiation on the energy of the photons for

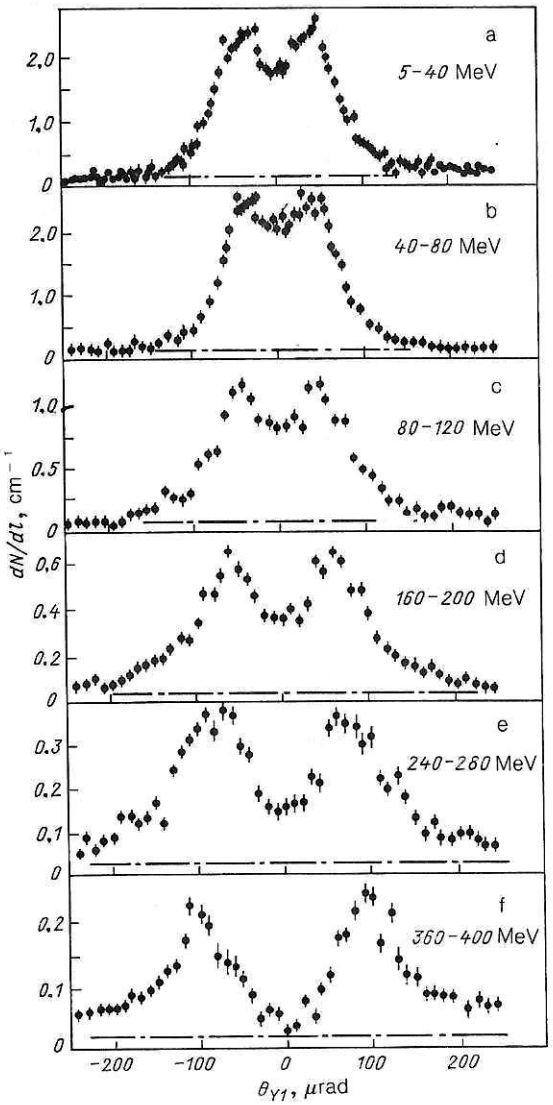

FIG. 3. Distributions of the number of photons for different energy ranges as functions of the positron angle of entry.

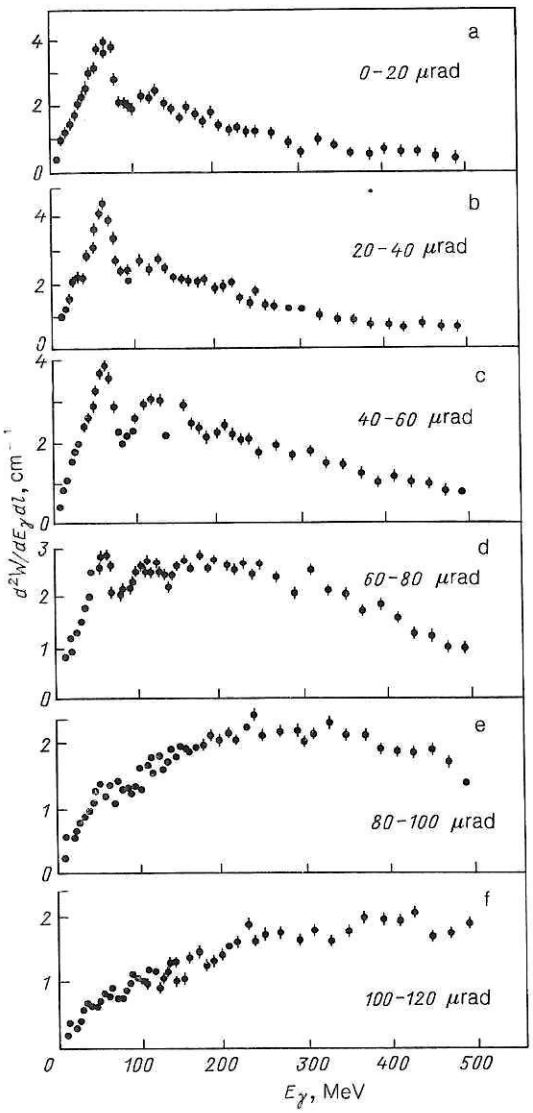

FIG. 4. Radiation spectral density as a function of the photon energy for different angles of entry of the positrons into the crystal.

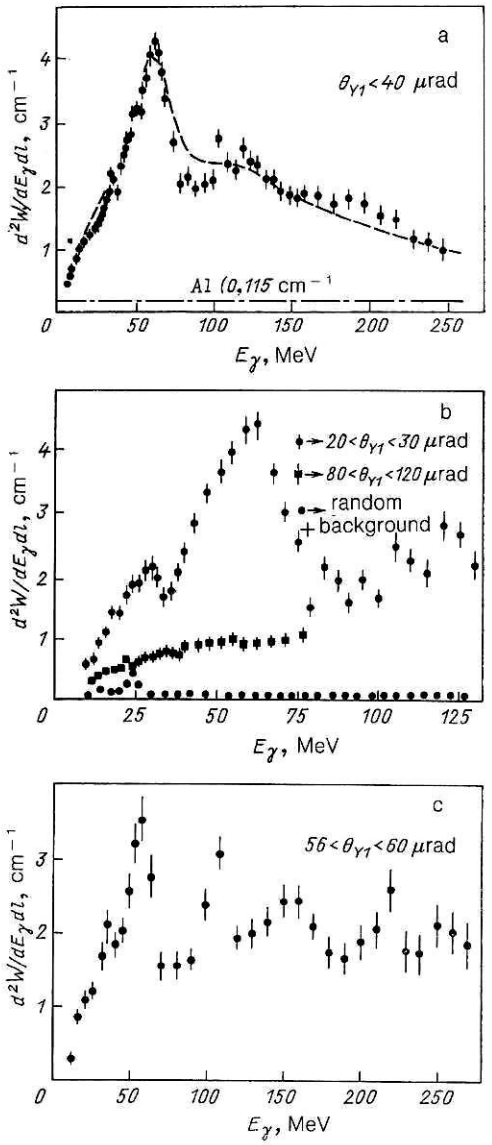

FIG. 5. Radiation spectral density as a function of the photon energy. Particles in the different intervals of entry angles shown in the figures were selected. The chain line shows the distribution obtained for the aluminum target, and the broken curve was calculated in accordance with Ref. 23; the dots show the background spectrum, which includes radiation from the matter of the facility and random coincidences with noise signals of the spectrometric tract.

particles in different ranges of angles of entry. The dependences in Fig. 4 show the dynamics of the transition from radiation when there is channeling (a, b) to radiation in the transition region of angles (c, d) and to coherent bremsstrahlung (e, f). Analyzing them, one can conclude that the radiation in the case of channeling is not a special case of coherent bremsstrahlung, and that the transition between these types of radiation occurs because of the disappearance of the peak associated with the channeling and the increase in the spectral density of the coherent bremsstrahlung in the region of higher photon energies (broad peak, Figs. 4d–4f). For channeled particles (Fig. 5) the radiation spectral density in the region of the maximum (60 MeV) is 37 times greater than the radiation spectral density in an amorphous target of equivalent thickness.

It follows from work done at CERN that the radiation spectral density exceeds the corresponding value obtained in the case of an unoriented target by about 24 times. The difference from our data can be attributed to the insufficient angular resolution of the facility built at CERN (about 60 μrad). This made it impossible to select channeled particles reliably, and therefore the observed spectrum was distorted by the radiation from particles that were not involved in the regime of planar channeling.

In our first studies a peak was observed (with a fairly large statistical error) in the radiation spectral density for photons with energy around 25 MeV. It follows from Fig. 5b, which shows the low-energy part of the radiation spectrum obtained in subsequent analysis, that the feature in the spectrum for this range at photon energy around 30 MeV does indeed exist and is not due to the background. The observed dependence of the intensity of the peak in the region of 30 MeV as the angle of entry of the positrons is varied from 20 to 120 μrad also indicates a connection of this peak with the investigated process.

As we noted in our early studies, a periodic structure appears in the radiation spectrum for particle entry angles near the critical value. This structure also appeared in the subsequent analysis for particles with angles of entry restricted to the range 56–60 μrad (Fig. 5c). Most of these particles are in a region near a plane of atoms during their motion within the crystal. In this region the potential differs from the parabolic dependence that describes the motion in the regime of stable planar channeling, and this can explain the change in the shape of the spectrum.

In the experiment the influence of the criteria for event selection on the absolute magnitude of the radiation effect was tested. It was found that for a 40% change of each of the main criteria the absolute magnitude of the effect changed by not more than 1.5–2% (in the region of γ rays with energy around 60 MeV). In the region of softer photons (around 30 MeV) the change in the effect was more appreciable—about 8%. For photons with energy above 100 MeV the change in the effect did not exceed 1%. It follows from these data that the random events, whose fraction changes when the selection criteria are changed, lie mainly in the region of photons with energy below 30 MeV.

We estimate the systematic error in the normalization of our data at the level 10%; it is largely determined by uncontrollable variations in the efficiency of the facility associated with the nonuniform load of the spectrometer. The data of measurements of the spectral density of the radiation in the case of an aluminum target (0.115 ± 0.01 cm^{-1}) agree with the calculation, which gives the value 0.12 cm^{-1}.

Comparisons with theoretical predictions

The first theoretical studies of Kumakhov[1] and the possibilities opened up for using a new type of radiation as an intense source of γ rays stimulated further theoretical studies in this field.[23] General problems of the theory of radiation produced in the case of channeling and in the transition region (several critical channeling angles) were analyzed. The experimental data available for high-energy particles[2] confirmed qualitatively the predictions of the theory, but they were not sufficiently detailed to test the quantitative conclusions of the theoretical studies and establish their validity for different channeling conditions.

The distribution of the radiation spectral density (Fig. 5a) agrees qualitatively with the distribution calculated the-

oretically. The observed dependence of the radiation spectral density in the region of its maximum as a function of the angle of entry of the positrons into the crystal (Fig. 4) and the distributions in Figs. 3a and 3b are an experimental confirmation of the theoretical predictions for the dependence of the radiation characteristics on the angle of entry for channeled positrons.

The dependence of the fine structure of the spectrum in the region of photon energies around 120 MeV on the entry angle of the particles (Figs. 4a–4c and Fig. 5a) requires the use of additional ideas about the mechanism of radiation at high harmonics in a nonparabolic potential. Analysis of the radiation spectrum at angles near the critical value (Fig. 5c) should also be helpful in determining more precisely the shape of the planar potential in the region near the bottom of the potential well.

Thus, we obtained the angular and energy dependences for the electromagnetic radiation produced when high-energy positrons pass through a silicon single crystal.

We showed that in the case of planar channeling of the positrons the spectral density of the radiation exceeds by 37 times the corresponding value for an amorphous target.

For the first time radiation in a wide range of angles of entry of the positrons relative to the direction of the crystal plane was investigated. This made it possible to obtain data on the dynamics of the transition from channeling radiation to coherent bremsstrahlung.

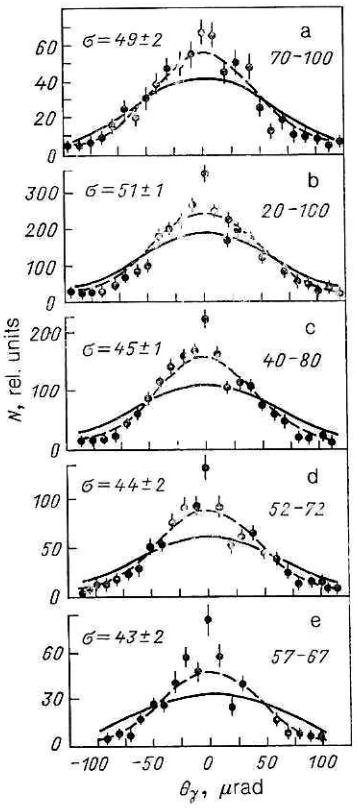

FIG. 6. Distributions of events with respect to the emission angles of the photons relative to the (110) plane. The range of positron entry angles is from -60 to $+60$ μrad. The numbers on the right are the limits of the interval of photon energies, and those on the left are the standard deviations of the curves; the broken curves are the results of approximating the experimental data by a Gaussian distribution, and the continuous curves are the calculated distributions of radiation from an amorphous target.

Angular distributions of photons radiated by positrons near the (110) plane

Figures 6–9 show the angular distributions of photons radiated by positrons in a silicon crystal for different angles of orientation relative to the crystallographic plane (110). The distributions have been plotted for different ranges of the photon energies.

Figure 6 gives the distributions of the angles of emission with respect to the crystallographic plane (110) of photons radiated by positrons with entry angles from -60 to $+60$ μrad. The rms deviation of the analogous calculated distribution from an amorphous target with allowance for the beam divergence is about 82 μrad, a value that appreciably exceeds the rms deviation of the experimental distributions (Figs. 6a–6e). Photons with energy around 60 MeV have the smallest angular spread (Fig. 6e), and this corresponds in our case to the maximum of the spectral density of the radiation obtained in the case of channeling.

Figure 7 shows the angular distributions of the photons radiated by positrons with angles of entry into the crystal in the interval 70–140 μrad. The distribution of the photons with energies 20–100 MeV (Fig. 7a) has a mean value shifted by about 50 μrad to smaller angles relative to the calculated distribution. To a large degree this can be explained by rescattering of the positrons with subsequent capture of them in the channeling regime, in which the probability of radiation in this range of photon energies is several times greater than the probability of radiation outside a channel. With increasing energy of the photons (Fig. 7b), the mean value of the experimental distribution approaches the mean value of the calculated distribution, and at energies 300–600 MeV the two values are approximately the same (Fig. 7c). As the energy of the photons increases, their angular spread decreases, and at energies 300–600 MeV, corresponding ap-

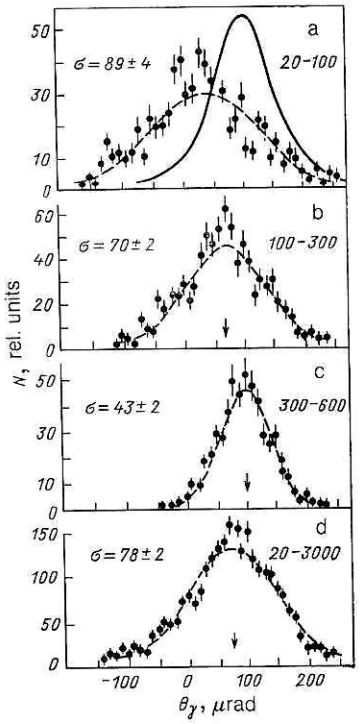

FIG. 7. The same as in Fig. 6. The positron entry angles are in the interval 70–140 μrad.

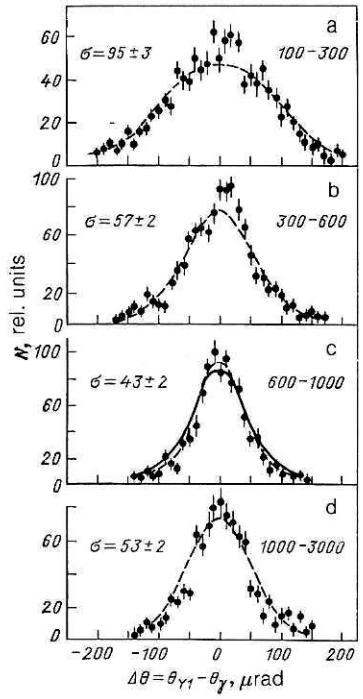

FIG. 8. Distributions of events with respect to the emission angles of the photons relative to the direction of the incident positrons. Events with entry angles in the interval 140–300 μrad were selected.

proximately to the maximum of the spectral density of the coherent bremsstrahlung for the given orientation, it is about 43 μrad, appreciably less than the angular spread of the radiation from an amorphous target.

Figure 8 shows the distributions of the photon angles of emission relative to the direction of the incident positrons. Events with positron emission angles in the interval 140–300 μrad were selected. It follows from comparison of the distributions (Figs. 8a–8d) that the values of their rms deviations depend on the energy of the photons. For given orientation of the positrons the greatest angular spread corresponds to photons with energy 600–1000 MeV, this range corresponding to the maximum of the spectral density of coherent bremsstrahlung. An analogous conclusion follows from comparison of the angular distributions corresponding to different intervals of energies of photons radiated by positrons with large angles of orientation (Figs. 9a–9c).

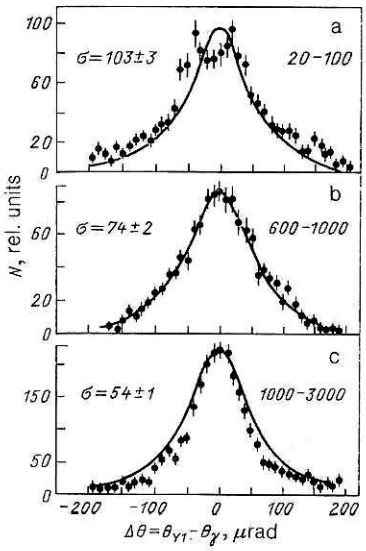

FIG. 9. The same as in Fig. 8. The positron entry angles are in the interval 300–1000 μrad.

The smallest angular spread corresponds to photons with energy 3000 MeV (Fig. 9c), and this also corresponds to the region of the maximum of the spectral density of the coherent bremsstrahlung.

Thus, the experimental data indicate that both in the case of spontaneous radiation in the presence of channeling and in the case of coherent bremsstrahlung the narrowest angular distributions correspond to photons with energies in the region of the maximum of the spectral density of the radiation.

3. INVESTIGATION OF THE RADIATION BY POSITRONS IN THE CASE OF AXIAL CHANNELING

For analysis of the data, events in which a photon with energy above 5 MeV was detected were selected. The sum of the energies of the photon and the secondary positron had to be equal to the energy of the particles in the beam. A silicon crystal of thickness 113 μm was oriented with the ⟨111⟩ axis parallel to the direction of the positron beam.

Orientation dependences

The orientation dependence characterizes the probability of radiation of a photon by a positron that enters the crystal at a definite angle. For axial channeling, in contrast to the one-dimensional case of planar channeling, the radiation probability depends on both angular variables (θ_X, θ_Y in a rectangular coordinate system or θ,φ in a polar coordinate system). The angle θ is measured from the direction of the crystal axis.

Figure 10 shows the distribution of the number of radiated photons with energy in the range 5–200 MeV as a function of the angle of entry of the positron into the crystal. It can be seen that there is a greater probability of radiation for particles that enter the crystal along a direction close to the ⟨111⟩ axis and the (110) and (112) planes.

Figure 11 shows the dependence of the number of radiated photons on the polar angle of entry of the positrons into the crystal. For particles with entry angle near zero the radiation probability is suppressed and reaches a maximum at entry angles near 150 μrad, this being a value somewhat greater than the critical angle of axial channeling (about 130 μrad). Thus, the maximum of the radiation probability is reached at the boundary of the region of axial channeling and is about 19 photons per 1 cm of crystal. For a crystal of thickness 113 μm the probability of radiation at the maximum is about 0.21. The probability of radiation of two photons is about 11% of the total number of photons. It must be borne in mind that double photons somewhat distort the measured radiation characteristics. However, the probability of detection of two photons depends on the response threshold of the photon spectrometer. Thus, for a threshold of 5 MeV the probability of superposition of two photons is 11%, whereas for a threshold of 20 MeV it is about 8%.

Figure 12 shows the dependences of the number of radiated photons (in different energy ranges) on the polar angle of entry of the positrons. It can be seen from the distributions that the probability of radiation of photons in all energy

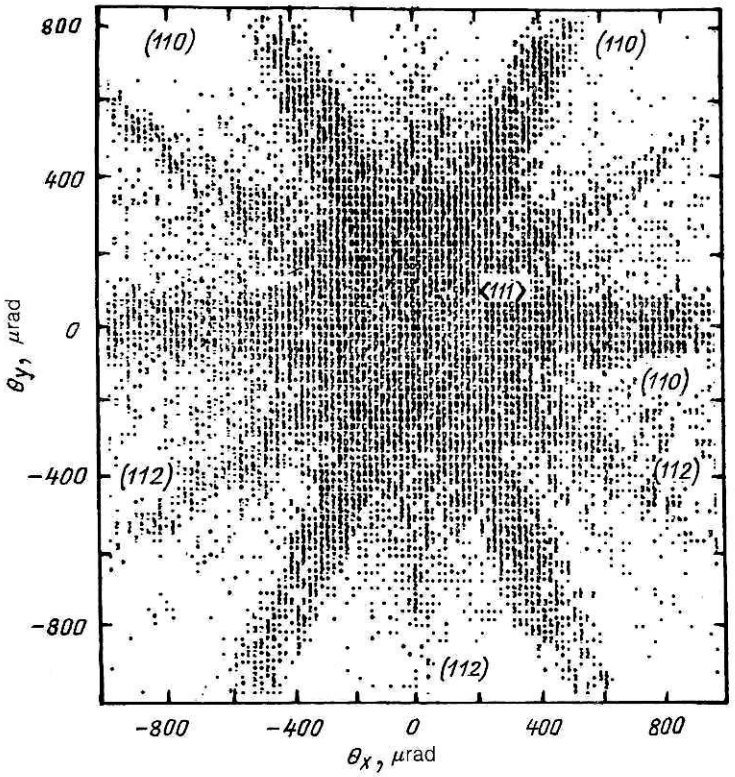

FIG. 10. Distribution of the number of radiated photons as a function of the angle of entry of the positrons into the crystal.

ranges has a minimum for positrons with small angles of entry into the crystal. Such behavior of the orientation dependences characterizes the dynamics of the motion of the positrons in the crystal in the case of axial channeling. The distributions in Fig. 12 are plotted without selection with respect to the azimuthal angle. It is obvious that the presence of crystallographic planes of different orders leads to a dependence of the radiation probability on not only the polar but also the azimuthal angle of entry of the positrons.

Figure 13 shows the analogous dependences for events in which the positrons have angle of entry not exceeding 60 μrad relative to the crystallographic plane (110), and Fig. 14 shows the same dependences for the weaker plane (112). The number of photons radiated in the energy range 5–500 MeV becomes constant at polar angles greater than 400 μrad, i.e., for angles less than 400 μrad the influence of the crystallographic axis on the radiation probability is appreciable. For large polar angles the probability of radiation of low-energy photons (Figs. 13a and 14a) becomes constant and is due to planar channeling of the positrons. For higher photon energies the influence of the axis and the neighboring planes extends to polar angles that exceed the opening of the spectrometer (Figs. 13b–13d and 14b–14d).

The data of the experiment make it possible to compare the radiation resulting from channeling by the planes (110) and (112). Figure 15 shows the distribution of the number of photons as a function of the angle of entry relative to the plane (112) for events corresponding to the maximum in the radiation spectral density (see Fig. 19). Particles with polar angle greater than 500 μrad, for which the influence of the

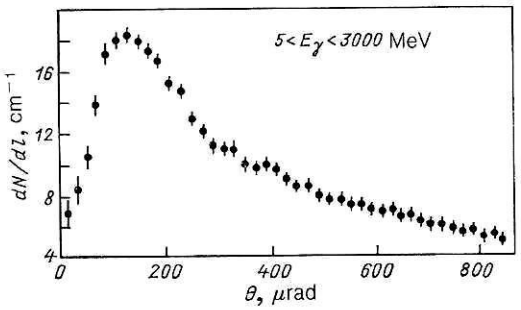

FIG. 11. Dependence of the number of radiated photons on the polar angle of entry of the positrons into the crystal.

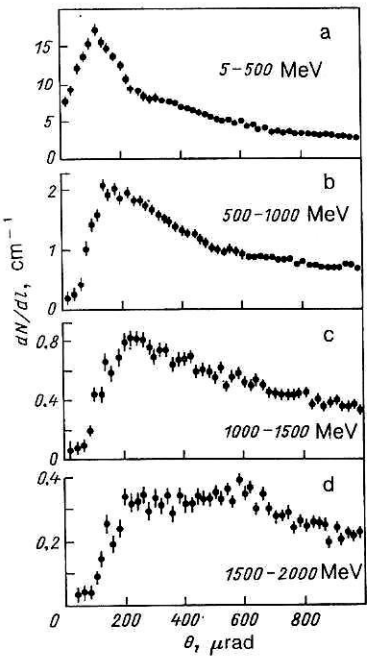

FIG. 12. The same as in Fig. 11 for γ rays in different energy ranges.

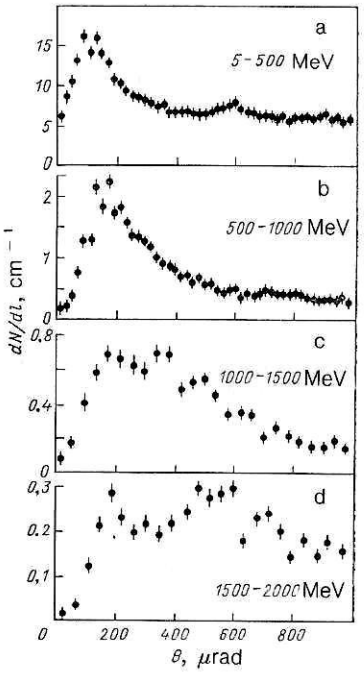

FIG. 13. The same as in Fig. 12 for positrons that entered the crystal near the (110) plane.

axis on the radiation probability becomes less significant, were selected. The distribution shows that the radiation probability for positrons channeled by the (112) plane is approximately two times less than for the case of the (110) plane, in fairly good agreement with the theoretical predictions. The theoretical value for the critical angle of channeling by the (112) plane is about 40 μrad, in good agreement with the width of the distribution in Fig. 15.

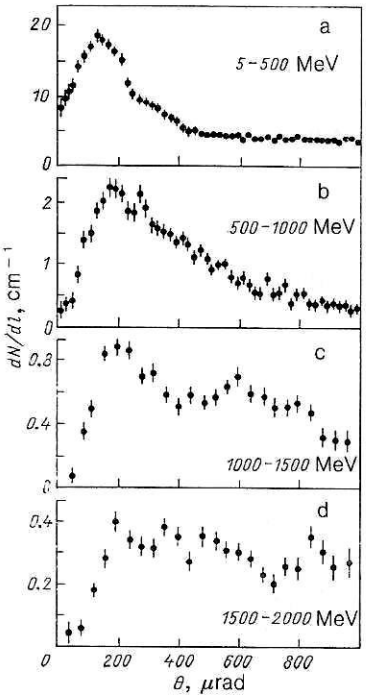

FIG. 14. The same as in Fig. 12 for positrons that entered the crystal near the (112) plane.

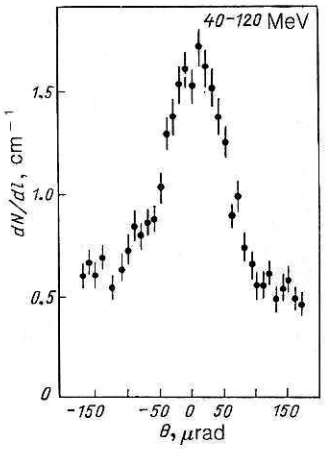

FIG. 15. Dependence of the number of radiated photons on the angle of entry of the positrons relative to the (112) plane.

Spectral density of the radiation

Figure 16 shows the dependence of the radiation spectral density on the photon energy for events with polar angle of entry into the crystal less than 80 μrad. The values of the radiation spectral density for axial and planar channeling of the positrons are approximately the same. However, for the axial case the region of photon energies in which the spectral density is maximal is somewhat broader. The broken line characterizes the spectral density of the radiation for the aluminum target.

The comparatively large aperture of the facility made it possible to obtain data on radiation in a wide range of angles—from angles corresponding to axial channeling to angles that ensure conditions of planar channeling.

Figures 17 and 18 show the dependences of the radiation spectral density on the photon energy for particles having different polar angles of entry. The events were selected in such a way that the angle of entry with respect to the crystallographic planes (110) (Fig. 17) and (112) (Fig. 18) did not exceed 60 μrad. The distributions in Figs. 17a and 18a show the spectral density of the radiation for positrons participating in axial channeling. These distributions are almost identical, and this shows that the characteristics of the radiation do not depend on the azimuthal angle within an angular cone with a width of about 100 μrad. The distribu-

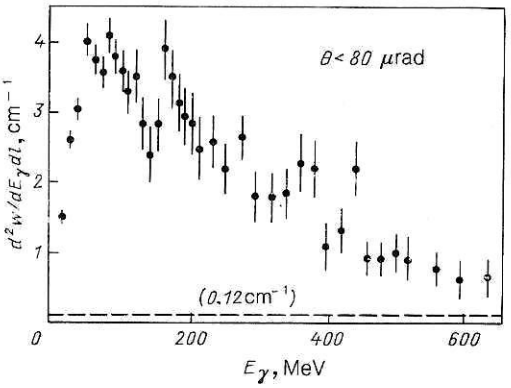

FIG. 16. Dependence of the radiation spectral density on the photon energy for axial channeling of positrons.

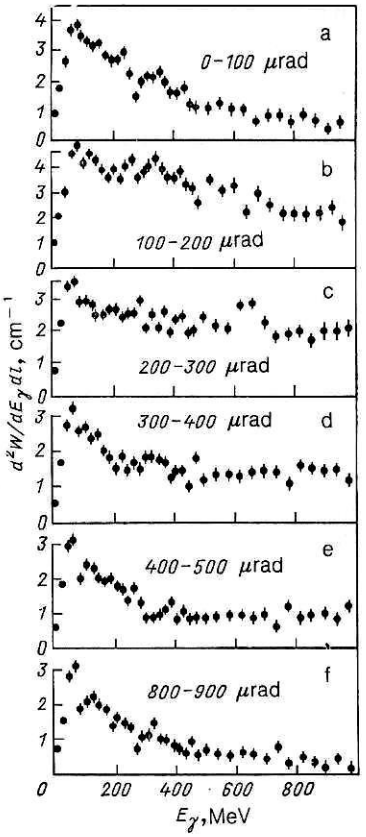

FIG. 17. Dependence of the radiation spectral density on the photon energy for different intervals of the polar angles of entry of the positrons into the crystal. Positrons that entered the crystal near the (110) plane were selected.

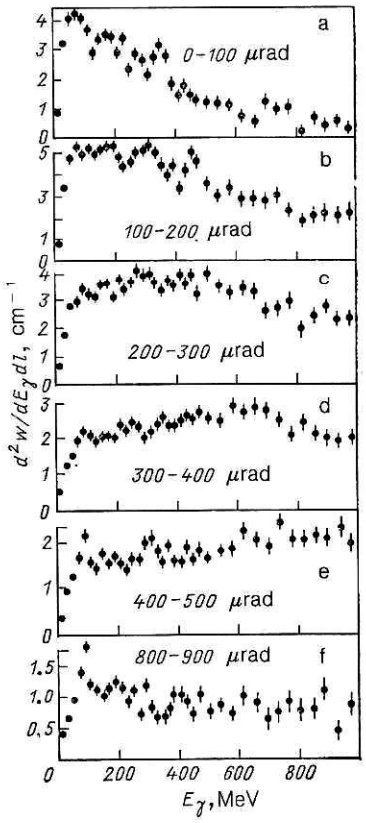

FIG. 18. The same as in Fig. 17 for positrons that entered the crystal near the (112) plane.

tion (b, c) corresponds to radiation in the region of angles transitional from an axis to a plane, and (d, f) to radiation of planar channeled positrons, in which a peak with energy corresponding to radiation in the presence of planar channeling can be seen. In the region of polar angles above 100 μrad, Figs. 17 and 18 differ appreciably. The influence of the axis and the neighboring planes is somewhat rather greater on the radiation spectrum of particles that enter the crystal near the (112) plane. Thus, for positrons with polar angle of entry greater than 800 μrad (Fig. 17) this influence becomes negligible, and the spectrum agrees well with the data that we obtained earlier for an isolated (110) plane. For positrons channeled by the (112) plane the influence of the axis and neighboring planes on the radiation spectrum extends to polar angles that exceed the opening of the spectrometer (Fig. 18f). This influence takes the form that the level of radiation with energy above 400 MeV appreciably exceeds the level for positrons channeled by the (110) plane (Fig. 17f). The value of the radiation spectral density for the amorphous target is about 0.1 cm^{-1}, a value that also differs appreciably from the radiation level (in Fig. 18f). These distributions show that the radiation spectral density depends on both the polar and the azumithal angle relative to the crystal axis.

Figure 19 shows the dependence of the radiation spectral density on the photon energy for particles with angles of entry into the crystal less than 40 μrad relative to the (112) plane and with polar angles of entry greater than 500 μrad. The spectral density for the chosen events is 15 times greater than the corresponding density for the aluminum target of equivalent width, in agreement with the calculation that uses the result of Ref. 23.

Figure 20 shows the dependence of the total radiative energy losses on the angle of entry of the positrons into the crystal. Events with photons in a wide range of energies were selected. The maximal energy loss due to radiation is reached at polar angles near 200 μrad, this exceeding somewhat the critical angle for axial channeling. This shape of the curve can be explained, first, by the fact that the radiation probability is maximal at entry angles near 150 μrad, and, second, by the fact that with increasing polar angle of entry of the positrons into the crystal the spectrum is shifted to the harder region of energies.

Thus, we obtained results that characterize the radiation produced when 10-GeV positrons pass through a silicon single crystal at small angles to the ⟨111⟩ axis. We showed that the spectral density of the radiation of axially

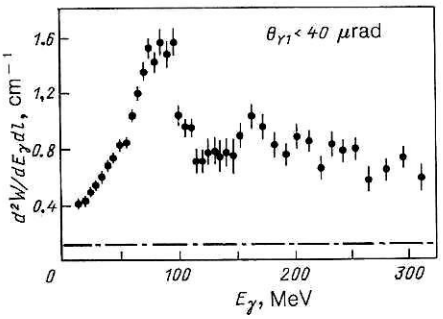

FIG. 19. Dependence of the radiation spectral density on the photon energy for positrons that entered the crystal near the (112) plane.

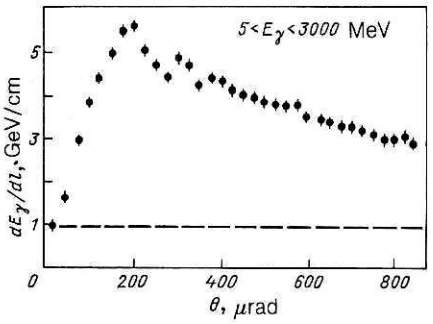

FIG. 20. Dependence of the total radiation energy losses on the polar angle of entry of the positrons into the crystal.

channeled positrons is 35 times greater than the corresponding value for an amorphous target.

We have given the characteristics of the radiation for a wide range of angles around the crystal axis, and we have also given data that characterize the total energy loss due to radiation.

The radiation of positrons in the case of axial channeling is not amenable to analytic calculation. Its interpretation requires a laborious numerical modeling of the more complicated motion of the positrons in the directions perpendicular to the crystal axis.

4. INVESTIGATION OF THE RADIATION BY ELECTRONS IN THE CASE OF AXIAL CHANNELING

The crystal was oriented in such a way that the direction of the crystallographic axis ⟨111⟩ coincided with the direction of the electron beam.

Orientation dependences of the radiation probability

The probability of photon radiation by electrons depends on the polar angle of entry of the electron relative to the crystallographic axis and on the azimuthal angle. Figure 21 shows the distribution of events in which an electron radiated a photon with energy from 10 to 600 MeV. The distribution clearly illustrates the influence of the ⟨111⟩ axis and (110) planes on the probability of photon radiation.

Figure 22 shows the dependences of the number of detected photons on the polar angle of entry of the electrons relative to the crystal axis ⟨111⟩ for different ranges of photon energies. Each point of the distribution has been normalized to the number of electrons in the solid angle corresponding to the interval of polar angles of entry. It can be seen from the figure that for channeled electrons ($\theta \leqslant 130$ μrad) the yield of photons is maximal. For "above-barrier" electrons ($\theta > 130$ μrad) the photon yield is much lower. In the energy range $0.01 \leqslant E_\gamma \leqslant 3$ GeV the maximal value is ~30 photons per 1 cm of crystal. The influence of the axis on the photon yield is still appreciable at entry angles of about 400 μrad. For larger angles the radiation level becomes constant and is largely determined by planar channeling of the electrons. An exception is the case of photons of high energies ($2 \leqslant E_\gamma \leqslant 3$ GeV, Fig. 22), for which the radiation probability is almost independent of the electron entry angle.

The comparison with data obtained for positrons of the same energy indicates differences in the dynamics of the motion of the electrons and positrons in the process of axial channeling. Thus, the maximal probability of photon radiation is reached for electron entry angles near zero (15–20

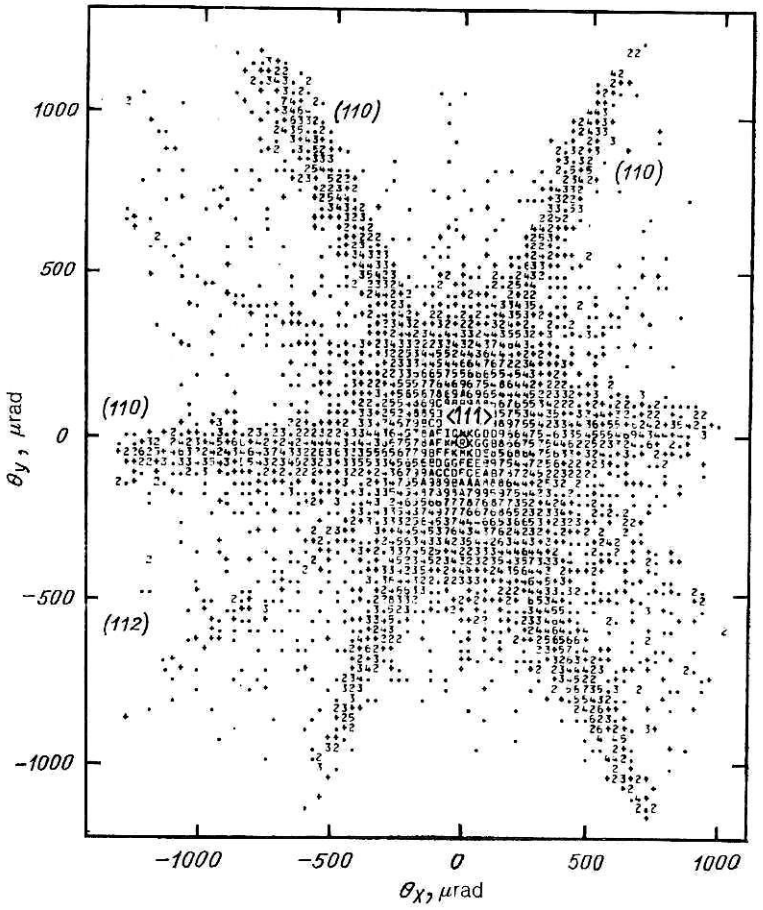

FIG. 21. Distribution of the number of events that were accompanied by radiation of photons with energy from 10 to 600 MeV as a function of the angle of entry of the electrons into the crystal; θ_x and θ_y are the projections of the polar angle of entry onto the abscissa and ordinate in a rectangular coordinate system.

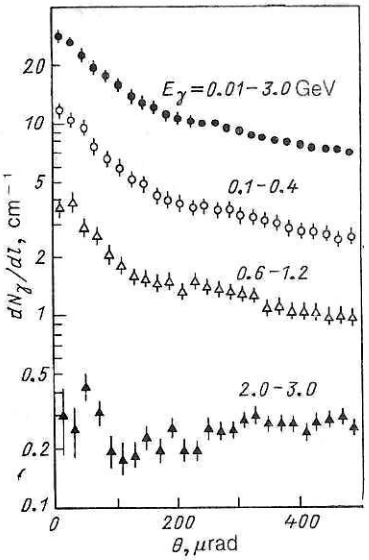

FIG. 22. Dependence of the number of detected photons on the polar angle of entry of the electrons into the crystal for different intervals of photon energies.

μrad, Fig. 22), whereas for positrons the maximal probability is reached at angles near the critical angle. This is explained by the fact that for entry angles near zero an electron can approach the axis in a region of large field gradients, whereas for positrons this occurs at entry angles near the critical angle.

Radiative energy losses of an electron

Figure 23 shows the results of measurement of the radiative energy losses of the electrons as functions of the polar angle of entry into the crystal. The curves were obtained under the same conditions as the data in Fig. 22.

Note that the maximal total radiative losses by an electron can be ≈ 10 GeV/cm. If events are selected on the basis of the criterion $0.1 \leqslant E_\gamma \leqslant 0.4$ GeV, then in this case the maximal radiative losses are ≈ 2.8 GeV per 1 cm of the crystal for channeled electrons. At the same time the energy losses by above-barrier electrons ($130 \leqslant \theta \leqslant 400$ μrad) are $\approx$600–900 MeV/cm.

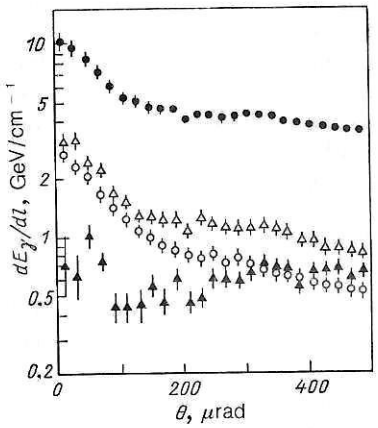

FIG. 23. Distribution of the radiation energy losses by the electrons as a function of the polar angle of entry into the crystal for different intervals of photon energies. The energy ranges corresponding to the experimental points are the same as in Fig. 22.

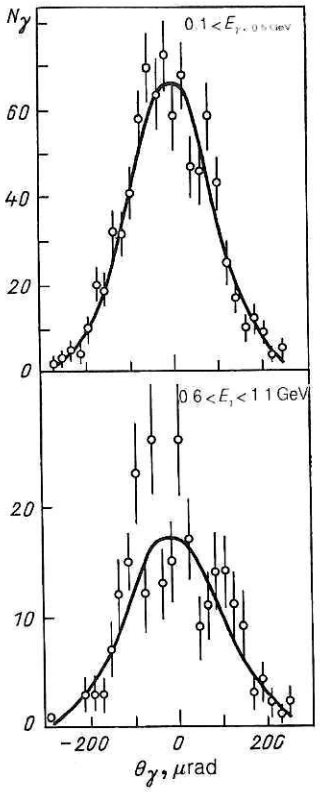

FIG. 24. Distribution of events with respect to the angles of emission of photons from the crystal for electrons with polar angles of entry less than 120 μrad relative to the ⟨111⟩ axis.

Angular distributions of the photons

Figure 24 gives the distributions of the events with respect to the angles of emission of photons from the crystal for electrons with polar angles of entry $\theta \leqslant 120$ μrad relative to the ⟨111⟩ axis. We measured the vertical projection of the photon angles of emission relative to the horizontal plane, obtaining the projection by reconstructing the point of conversion of the photon into an electron–positron pair in the drift chamber with a built-in converter. The ⟨111⟩ axis lay in the horizontal plane in this case. The continuous curve is the result of approximation of the experimental data by a Gaussian distribution. For events selected by the condition $0.1 \leqslant E_\gamma \leqslant 0.5$ GeV, the width of the rms deviation is 105 ± 8 μrad, and for events in which the photon energy was in the interval $0.6 \leqslant E_\gamma \leqslant 1.1$ GeV we obtained $\sigma = 115 \pm 12$ μrad. It can be seen from the figure that the photons radiated in the process of axial channeling of the electrons are scattered into a cone with opening angle approximately equal to the critical angle for channeling, this being somewhat broader than the bremsstrahlung cone for an amorphous body of the same thickness.

Radiation spectral density

Figure 25 shows the distribution of the radiation spectral density as a function of the photon energy for electrons in different ranges of entry angles. These distributions have also been normalized to the thickness of the crystal and to the number of electrons in the corresponding range of entry angles. The broken lines show the level of the spectral density of bremsstrahlung from an aluminum target.

The data illustrate the dependence of the spectral den-

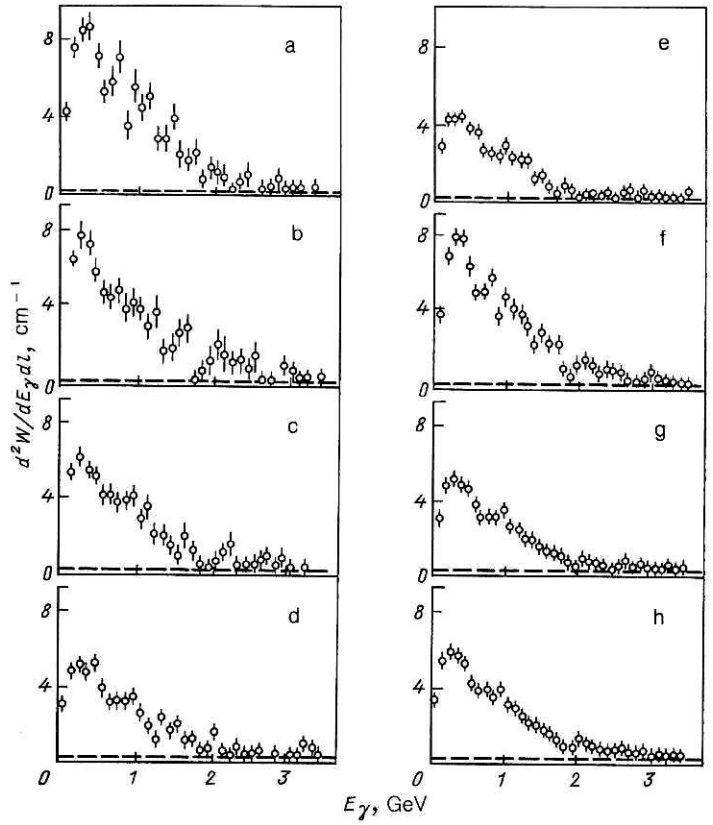

FIG. 25. Dependence of the radiation spectral density on the photon energy for different angles of entry θ, μrad, of the electrons into the crystal: a) 0–40, b) 40–60, c) 60–80, d) 80–100, e) 100–120, f) 0–60, g) 60–120, h) 0–120.

sity of the radiation on the angle of entry of the electron into the crystal. Electrons with entry angles $\theta < 40$ μrad radiate most strongly.

The maximum of the spectral density is in the region of photon energies around 250 MeV. Its value exceeds the level of radiation in an amorphous body by about 70 times. Attention should be drawn to the fact that the distribution of the spectral density in the case of axial channeling of electrons is appreciably broader (by about three times) and approximately two times higher (at the maximum) than the analogous distribution for positrons.

The data obtained in the present study agree qualitatively with the theoretical ideas developed in Ref. 23.

The analytic methods of calculating the radiation spectral density obtained in these studies are based on model representations and do not take into account some real features of the averaged potential of the crystallographic axes,

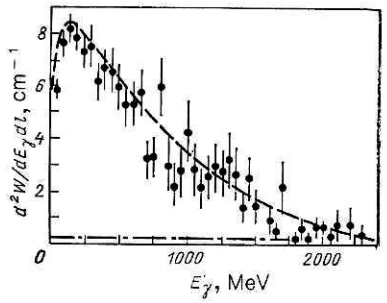

FIG. 26. Radiation spectral density of 10-GeV electrons. The broken curve is the result of a calculation made by means of modeling; the chain line is the radiation level in an aluminum target of equivalent width. The sample was ⟨111⟩ Si of thickness 41 μm, $\theta < 100$ μrad.

for example, its asymmetry. Allowance for the experimental conditions in these calculations lead to still greater difficulties. Data on the radiation spectral density for 10-GeV electrons obtained by modeling the paths of the motion in the real averaged potential of the crystal axes agree satisfactorily with the experimental results (Fig. 26).

5. RADIATION PRODUCED IN THE CASE OF PLANAR CHANNELING OF ELECTRONS

Before the present investigations, the electromagnetic radiation by electrons of ultrarelativistic energies in the process of planar channeling had hardly been studied. In this paper we give the results of the experimental investigation of the radiation by 10-GeV electrons moving along (110) planes.

The crystal was oriented with the (110) plane parallel to the direction of the beam. The disorientation with respect to the ⟨111⟩ crystallographic axis was 0.5°. The angles of entry (and exit) of the electrons into the crystal were measured relative to the (110) plane. These angles had the value zero when the (110) crystallographic plane and the velocity vector of the electrons were parallel.

Orientation dependences and radiative energy losses of the electrons

Figure 27 gives the distributions of the number of detected photons as a function of the angle of entry of the electrons into the crystal relative to the (110) plane obtained for different energy ranges of the photons. The distributions are reduced to unit length of the crystal, and each of their points was normalized to the number of electrons in the corresponding interval of entry angles. It can be seen from the figure that an orientation dependence of the photon yield is

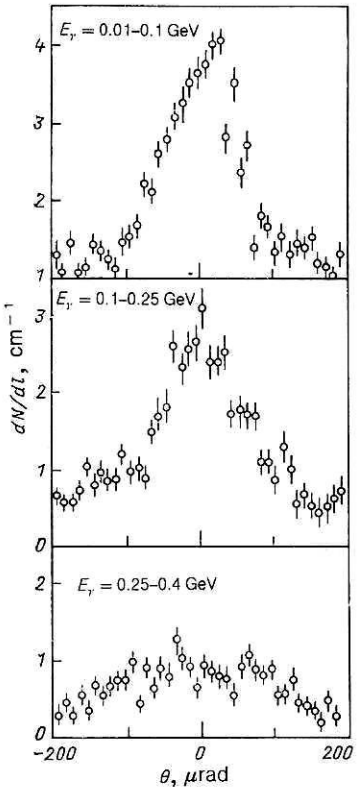

FIG. 27. Distribution of the number of detected photons as a function of the angle of entry of the electrons into the crystal relative to the (110) plane for different intervals of photon energies.

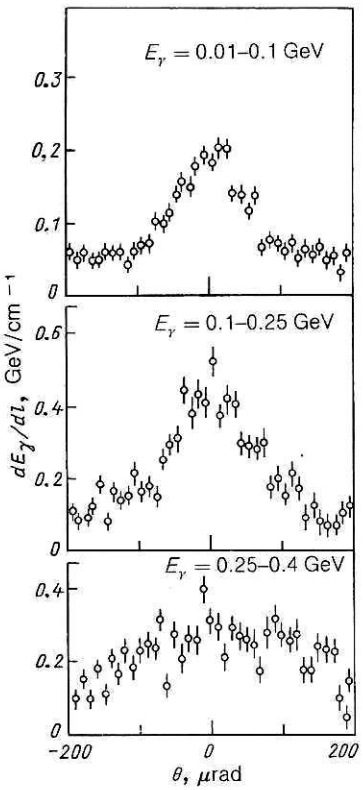

FIG. 28. Distribution of the radiation energy losses of the electrons as function of the angle of entry with respect to the (110) plane for different intervals of photon energies.

clearly manifested only for photon energy below 250 MeV. For higher energies the orientation effect is manifested weakly.

Figure 28 gives the results of measurement of the radiation energy losses of the electrons as functions of the angle of entry into the crystal in the same ranges of photon energies and under the same conditions as for Fig. 27. The distributions of Figs. 27 and 28 have similar shapes. However, the

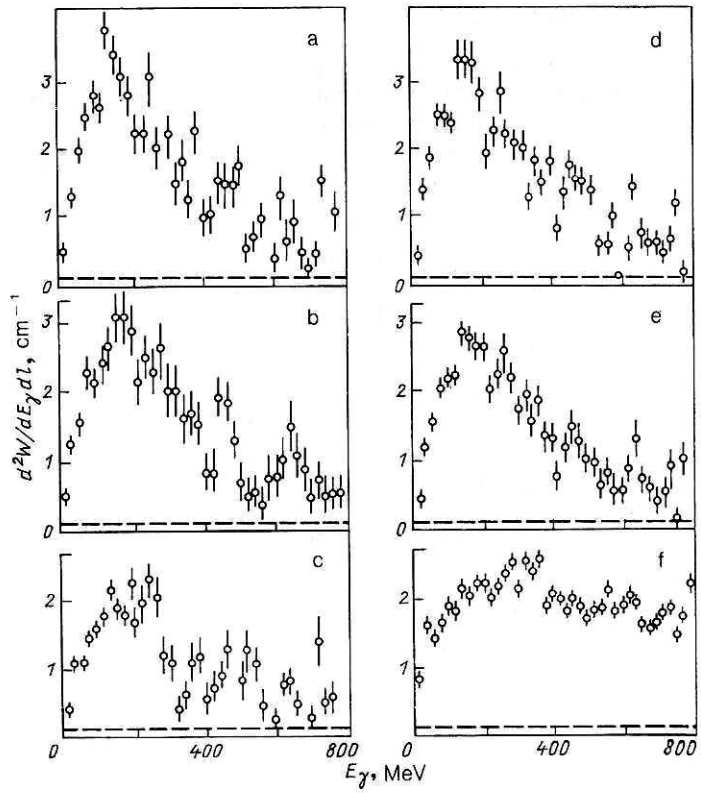

FIG. 29. Distribution of the radiation spectral density as a function of the photon energy for different intervals of the angle of entry, θ, μrad, of the electrons into the crystal relative to the (110) plane: a) 0–20, b) 20–40, c) 40–60, d) 0–30, e) 0–60, f) 0–100.

number of photons decreases with increasing energy of the photons, while the energy losses by the electrons are increased somewhat. It follows that the mean energy losses by the electrons vary little in the considered energy ranges of the photons and are about 200 MeV/cm.

Comparison of the distributions in Fig. 27 with the analogous data obtained for positrons indicates a difference between the dynamics of motion of the electrons and positrons in the process of planar channeling. The maximum of the distribution for the electrons is at entry angle θ equal to zero, whereas for the positrons the distributions have two maxima, which are reached at entry angles near the critical angle of planar channeling (about 60 μrad at electron energy 10 GeV).

Figure 29 shows the distribution of the radiation spectral density as a function of the photon energy for different ranges of angles of entry of the electrons into the crystal. The conditions of normalization of these distributions are the same as for the distributions of Fig. 27 (however, in Fig. 29f the values of the spectral density must be multiplied by 10^{-1}, and the spectral density of bremsstrahlung from an amorphous target is 0.113 cm^{-1}). The broken lines show the level of the spectral density of bremsstrahlung from an amorphous target of similar thickness. The electrons radiate most strongly in the range of entry angles $0 \leqslant \theta \leqslant 20$ μrad. In this case the maximal value of the radiation spectral density is reached at $E_\gamma = 130$ MeV. It exceeds the level of bremsstrahlung from an amorphous target by 28 times. The data obtained at CERN in an investigation of radiation by electrons channeled in a planar channel give a similar excess of the spectral density by about 14 times. The difference from our result can be explained by the insufficient angular resolution of the facility at CERN.

The distributions of the spectral density (Fig. 29) are about three times broader than the corresponding dependences obtained for positrons. These differences are explained by the different nature of the interplane potential for electrons and positrons.

Angular distributions of the photons

Figure 30 gives the distributions of the events with respect to the angles of emission of the photons from the crystal for different ranges of electron entry angles. The vertical projection of the angles of emission of the photons relative to the crystallographic plane (110), which coincided with the plane of the horizon, was measured. The continuous curves show the result of approximation of the experimental data by a Gaussian distribution.

The distribution of events selected on the basis of the condition $\theta \leqslant 20$ μrad, for which the standard deviation is $\sigma = 75 \pm 7$ μrad, has the smallest width. Under the condition $20 \leqslant \theta \leqslant 40$ μrad we have $\sigma = 80 \pm 8$ μrad, and for $40 \leqslant \theta \leqslant 60$ μrad we have $\sigma = 86 \pm 8$ μrad.

Thus, in our studies we have obtained experimental data that characterize the radiation produced in processes of axial and planar channeling of 10-GeV electrons in a silicon single crystal of thickness 41 μm. We have given the characteristics of the electromagnetic radiation for different angles of entry of the electrons into the crystal, and also data that characterize the radiation energy losses. The angular characteristics of the radiation have been measured for the first time.

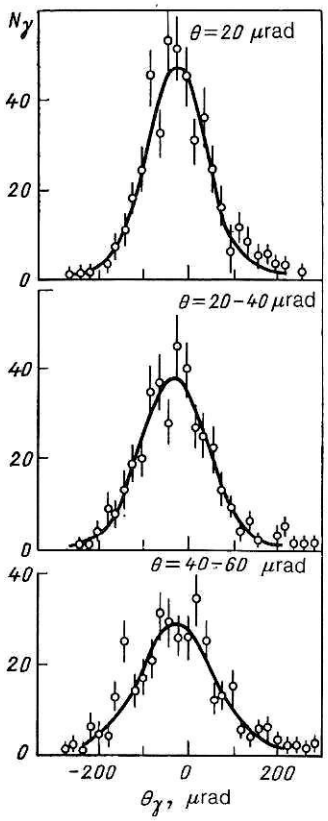

FIG. 30. Distribution of events with respect to the angles of emission of the photons from the crystal for different intervals of the angles of entry θ of the electrons.

We have shown that the spectral density of the radiation by the electrons in the process of planar channeling exceeds the spectral density of bremsstrahlung from an amorphous target by 28 times, and in the case of axial channeling by 70 times. Our data agree with the theoretical considerations of Ref. 23.

6. INVESTIGATION OF COHERENT BREMSSTRAHLUNG FROM RELATIVISTIC ELECTRONS AND POSITRONS IN THIN SILICON SINGLE CRYSTALS

The theory of coherent bremsstrahlung, developed in studies of Ter-Mikaélyan, Uberall, and others, has been worked out fairly fully and has reliable experimental confirmation for angles of entry of the particles into the crystal that are much greater than the critical angle for channeling (the Lindhard angle). However, because of the lack of systematic experimental data the question of the limits of applicability of the theory at small angles of orientation comparable with the Lindhard angle remains open.

Figure 31 shows the dependences of the number of emitted photons on the angle of entry of positrons into a silicon crystal of thickness 113 μm relative to the crystallographic plane (110). It can be seen that in the case of planar channeling the number of photons is approximately an order of magnitude greater than the number of photons generated in the case of coherent bremsstrahlung.

The broken lines give the corresponding dependences obtained using an aluminum target. In the interval of energies 10–80 MeV the maximum of the photon yield corresponds to positron entry angles within the Lindhard angle, which in our case was about 65 μrad. At a higher energy of

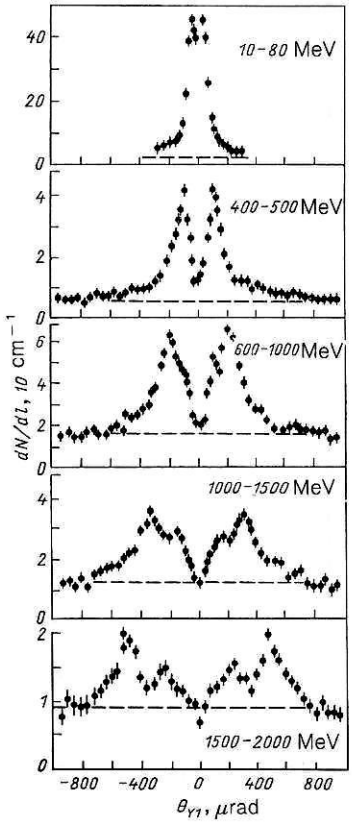

FIG. 31. Distribution of the number of photons for different energy intervals as a function of the positron entry angle.

the photons the maximum of their yield is determined by the coherent bremsstrahlung and is shifted to larger angles.

The crystal was oriented with the (110) plane parallel to the direction of the beam. The angle between the beam and the ⟨111⟩ axis of the crystal was about 0.5°.

Figure 32 gives the rms values of the angles of scattering of the positrons in the crystal as functions of their orientation relative to the (110) plane. In both cases the positron scattering angles have maxima at angles of entry into the crystal near the Lindhard angle and are about two times larger than the scattering angles in the case of an amorphous target.

Figures 33–36 give the dependences of the radiation spectral density on the photon energy for different ranges of

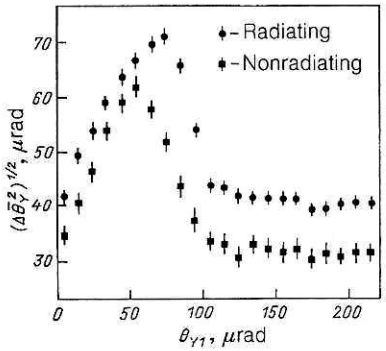

FIG. 32. Dependence of rms values of the scattering angles for positrons in silicon of thickness 113 μm on the orientation of the positrons relative to the (110) plane.

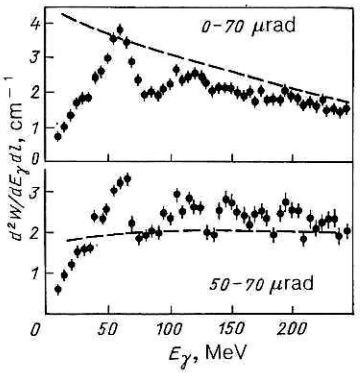

FIG. 33. Dependence of the radiation spectral density on the photon energy for different angles of entry of the positrons into the crystal relative to the (110) plane. The broken curve is the result of calculations in accordance with the theory of coherent bremsstrahlung.

the angle of entry relative to the (110) plane.

It can be seen from the comparison of the theory with the experiment that for positron entry angles within the Lindhard angle the theoretical curve differs qualitatively from the experimental data.

In Fig. 34 the continuous curve represents the calculation of the spectral density of the coherent bremsstrahlung obtained with allowance for the experimental values of the angles of multiple scattering (Fig. 32), and the broken curve gives the result of the calculation with multiple-scattering angles determined as for an amorphous target. It can be seen that in the first case the agreement of the calculated values with the experiment is somewhat better. The experimental values of the spectral density of the coherent bremsstrahlung for positron orientation angles in the intervals 70–80 and 80–100 μrad (Fig. 34) in the low-energy part of the spectrum are 20–30% greater than the theoretical values, and this is probably due to the contribution to the experimental data from the radiation of above-barrier particles and the radiation of particles trapped in the channeling regime after rescattering. This excess of the experimental data over the calculated values can be traced to values of the angle of entry into the crystal approximately equal to two Lindhard angles (Figs. 35a and 35b). For positron orientation angles greater than two Lindhard angles (Figs. 35c–35e and 36) the calculations in accordance with the theory of coherent bremsstrahlung agree well with the experimental data.

We give below the results of experimental investigation

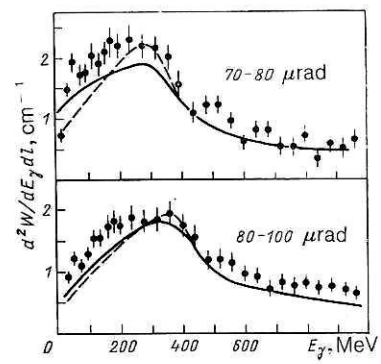

FIG. 34. The same as in Fig. 33 (see the text).

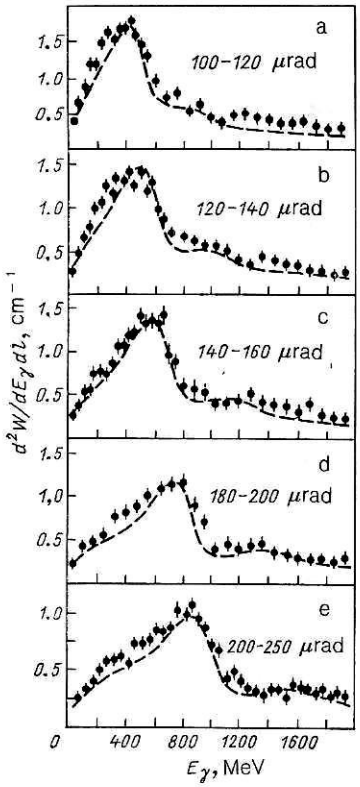

FIG. 35. The same as in Fig. 33 for positrons with angles of entry into the crystal greater than the Lindhard angles.

of the radiation of 10-GeV positrons and electrons moving at small angles relative to the (110) plane and ⟨111⟩ axis in a silicon single crystal.

To generate photon emission by positrons a silicon target of thickness 113 μm was used. The thickness of the target for the investigation of the electron radiation was 41 μm. According to our estimates, the systematic error in the measurements, determined largely by the instability of the load on the photon spectrometer, was about 10%. The experimental results are normalized to one incident particle and converted to a crystal of thickness 1 cm.

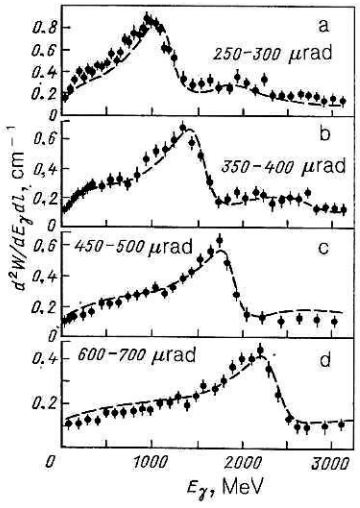

FIG. 36. The same as in Fig. 33 for positrons with large angles of entry into the crystal.

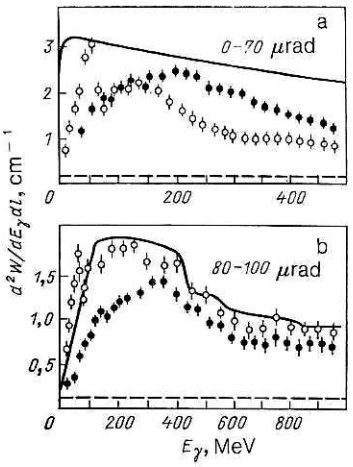

FIG. 37. Radiation spectral density of electrons (black circles) and positrons (open circles) as a function of the photon energy. The continuous curve is the result obtained in the theory of coherent bremsstrahlung; the broken line shows the spectral density of bremsstrahlung from an aluminum target.

Figures 37–39 show the spectral density of the radiation by electrons and positrons with different angles of entry θ_γ relative to the (110) plane. The angles of entry relative to the ⟨111⟩ axis were in the interval 500–1000 μrad.

The experimental spectra of the radiation by electrons and positrons with entry angles θ_γ in the intervals 0–70 and 80–100 μrad (Fig. 37) differ qualitatively in the low-energy part, both from each other and from the calculated spectra. The excess of the experimental values of the spectral density of the radiation by positrons in the interval 80–100 μrad over the theoretical values can be explained by the capture of particles into the channeling regime as a result of multiple scattering with subsequent radiation.

From a photon radiation of 100 MeV and above the positron radiation can be satisfactorily described by the theory of coherent bremsstrahlung, whereas the electron radiation is suppressed to a photon energy of 300–400 MeV; this difference may be due to the unequal influence of the ⟨111⟩ axis on the motion of the electrons and positrons before the radiation. For values of θ_γ in the intervals 100–150 and 150–200 μrad (Fig. 38) the experimental spectra of the electron and positron radiation agree with the calculated spectra to within the accuracy of the measurements. At large orientation angles (200–250, and 250–300 μrad, Fig. 39) the re-

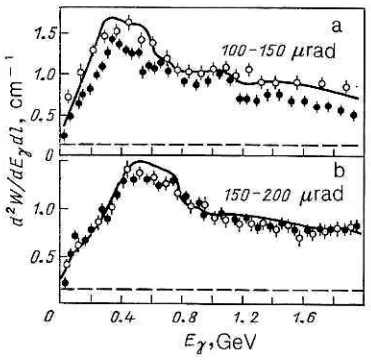

FIG. 38. The same as in Fig. 37 for particles with entry angles up to three Lindhard angles.

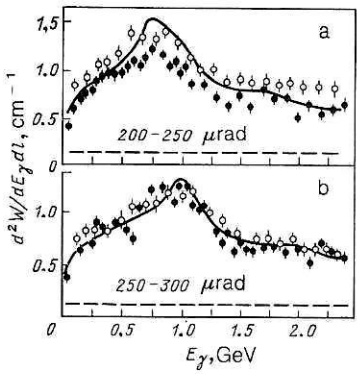

FIG. 39. The same as in Fig. 38 for particles with large angles of entry into the crystal.

sults of the calculation in accordance with the theory of coherent bremsstrahlung agree with the experimental data.

7. INVESTIGATION OF THE RADIATION BY 10-GeV ELECTRONS IN THICK SILICON AND GERMANIUM CRYSTALS

The experimental investigations of the predicted spontaneous radiation by relativistic electrons and positrons demonstrated the appreciable growth of the spectral density of the radiation by charged particles passing through a crystal along one of the principal crystallographic directions.

Below we give the results of investigation of the radiation by 10-GeV electrons that passed through silicon single crystals of thicknesses 0.8, 3.0, and 10 mm and a germanium single crystal of thickness 0.5 mm at small angles to the direction of the ⟨111⟩ crystallographic axis.

Investigation of the passage of relativistic electrons through thick single crystals

The results of investigation of the dynamics of motion of 10-GeV electrons in a thin (41 μm) silicon single crystal showed that particles incident on the crystal at small angles to the axis undergo strong scattering in directions perpendicular to the direction of the crystallographic axis. Electrons incident on the crystal at angles near the Lindhard angle undergo the greatest scattering in a thin single crystal. Figure 40 shows the rms angle of multiple scattering of electrons that passed through silicon single crystals of thickness 0.8 and 3.0 mm as a function of thr polar angle of entry relative to the axis (in units of the rms angle of multiple scattering in an amorphous target). The broken curve corresponds to the case of a thin crystal. It can be seen from the figure that in the

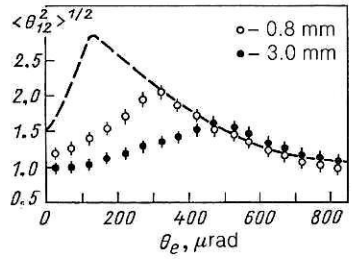

FIG. 40. Dependence of the rms angle of multiple scattering of electrons that passed through thick silicon single crystals (in units of the rms angle of multiple scattering in an amorphous medium) on the polar angle of entry relative to the axis.

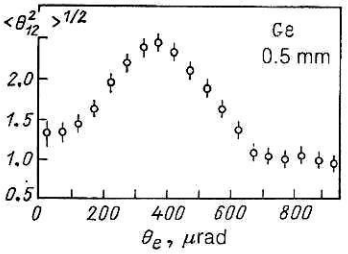

FIG. 41. Dependence of the rms angle of multiple scattering of electrons that passed through a germanium single crystal of thickness 0.5 mm on the polar angle of entry relative to the ⟨111⟩ axis.

samples of thickness 0.8 and 3.0 mm the maximal scattering occurs for electrons with angles of entry relative to the axis appreciably greater than the critical Lindhard angle. The analogous distribution for a germanium single crystal of thickness 0.5 mm is shown in Fig. 41. The displacement of the maximum in the distributions may indicate that in these samples some of the above-barrier particles are involved in the channeling process. Such an effect could arise because the angle between the direction of the axis and the velocity of the particle is reduced (at a certain depth in the crystal) by multiple scattering below the critical value. In this case dechanneled and above-barrier particles can be captured into the channeling process (so-called volume capture). The process of redistribution of the stream of particles that passed through the silicon single crystal of thickness 0.8 mm at small angles to the axis was particularly interesting. Figure 42 gives the distribution of the vertical projection of the angles of exit, θ_{Y2}, of the electrons from the single crystal for events with entry angles θ_{X1} from -150 to $+150$ μrad. The figure illustrates the influence of a chain of atoms on the motion of particles in thick single crystals, this leading to a redistribution of the particles with respect to the transverse energy.

Radiation by electrons in thick crystals

The main aim of the experiment was to investigate the spectral characteristics of the radiation from channeled particles. The results given above show that the spectral density of the radiation by electrons that passed through a thin silicon single crystal in the regime of axial channeling has a maximum at a photon energy around 200 MeV and in this

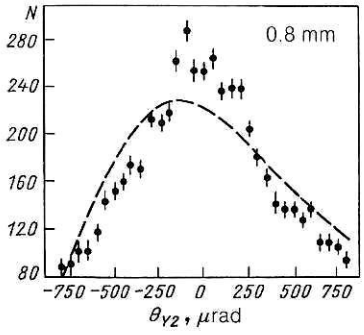

FIG. 42. Vertical projection of the angles of exit of electrons from a silicon single crystal of thickness 0.8 mm. The broken curve corresponds to the projection of the angles of entry for the same events (for which the angle of entry in the horizontal projection lies in the interval from -150 to $+150$ μrad).

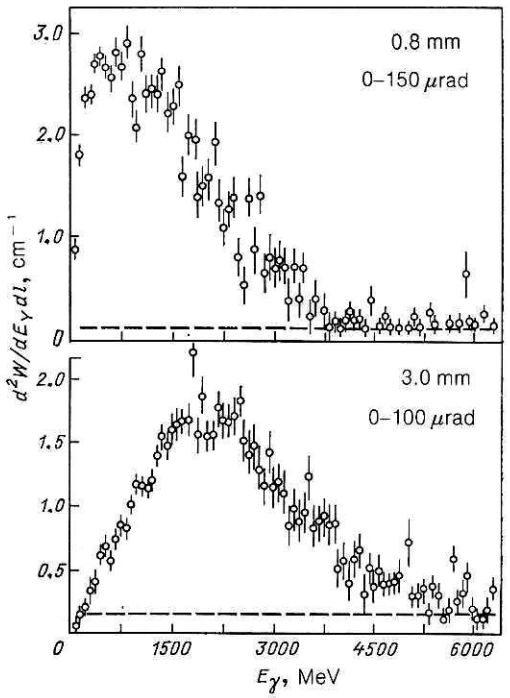

FIG. 43. Experimentally measured radiation spectral density in silicon crystals. The broken line shows the spectral density of the radiation from aluminum of the same thickness.

region exceeds the corresponding value for an amorphous target by about 70 times. In thicker crystals the multiple scattering associated with the thermal vibrations of the lattice atoms and scattering by electrons and defects of the crystal disrupts the regime of stable motion of the particles in the channels, and this leads to dechanneling. On the other hand, in the case of motion of particles along a chain of atoms the probability of radiation is appreciably greater than in amorphous matter. This has the consequence that in thick crystals several photons can be radiated by a single electron, and these were recorded by the photon spectrometer as a single photon with the total energy. In this connection, the spectral density of the radiation measured experimentally in our case for the investigated samples was integrated over several photons. Such distributions for silicon single crystals of thickness 0.8 and 3.0 mm are shown in Fig. 43. The analogous distribution for a silicon single crystal of thickness 10 mm is shown in Fig. 44.

Figures 45 and 46 show the experimentally measured

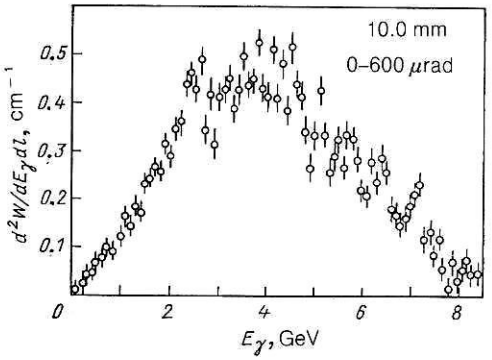

FIG. 44. Experimentally measured spectral density of the radiation in a silicon single crystal of thickness 10 mm.

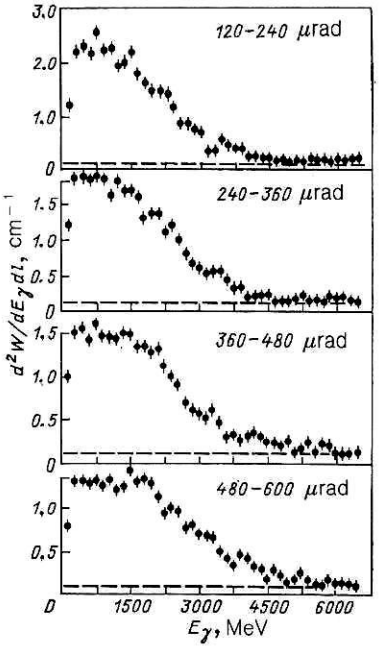

FIG. 45. Experimentally measured radiation spectral density of electrons in a silicon crystal of thickness 0.8 mm for events with different angles of entry relative to the axis.

spectral density of the radiation for a silicon single crystal of thickness 0.8 mm and for a germanium single crystal of thickness 0.5 mm for events with different angles of entry relative to the axis. These distributions illustrate the fact that with increasing angle between the incident beam of the electrons and the direction of the axis the energy losses vary weakly. Nevertheless, there is a certain broadening of the distributions with a simultaneous decrease of the radiation intensity. This can apparently be attributed to an increase of the contribution to the experimentally measured radiation spectral density from the high-energy bremsstrahlung by

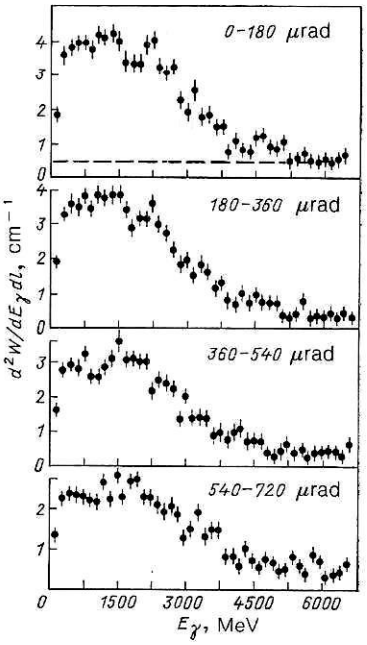

FIG. 46. Experimentally measured radiation spectral density of electrons in a germanium crystal of thickness 0.5 mm for events with different angles of entry relative to the axis.

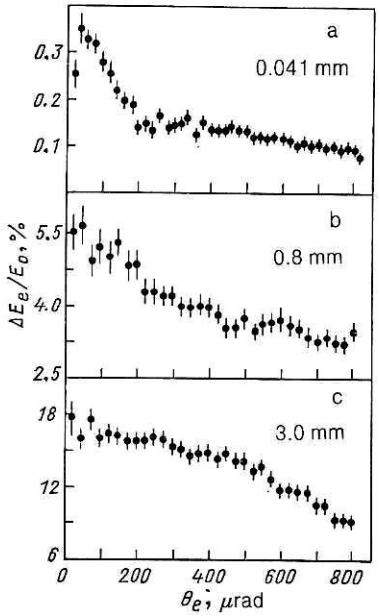

FIG. 47. Dependence of the mean relative energy losses of electrons that passed through silicon single crystals of different thicknesses on the polar angle of entry of the particles relative to the crystal axis.

above-barrier electrons with a simultaneous decrease of the contribution from the channeled particles that have the greatest probability of radiation and, therefore, are most strongly distorted by the detection of several photons.

Figure 47a gives of the mean energy losses of electrons that passed through a thin silicon single crystal as a function of the polar angle of entry relative to the axis. The dependence shows that the mean relative energy losses of electrons within the critical angle for channeling (about 130 μrad) are about 0.28%, while the above-barrier losses are about 0.12%. The analogous distributions for the single crystals of thickness 0.8 and 3.0 mm are shown in Figs. 47b and 47c. These distributions are characterized by a weaker orientation dependence of the mean relative energy losses of the electrons. It can be seen that for crystals of thickness 0.8 and 3.0 mm the mean relative energy losses of the electrons near the direction of the axis are about 5.1 and 16.3%, respectively. For the silicon sample of thickness 10 mm the mean relative energy losses of the particles reach about 30%. The distribution that characterizes the mean relative energy losses of the electrons in the germanium single crystal of thickness 0.5 mm is shown in Fig. 48. It follows from the figure that 7–8% of the energy of the primary beam that passed through the germanium crystal at small angles relative to the direction of the ⟨111⟩ crystallographic axis was transformed into

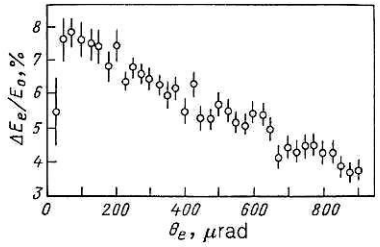

FIG. 48. Dependence of the mean relative energy losses of the electrons in a germanium single crystal of thickness 0.5 mm on the polar angle of entry into the target with respect to the ⟨111⟩ axis.

energy of electromagnetic radiation. For comparison, we note that the corresponding value measured under the same experimental conditions for an amorphous aluminum target of thickness 0.95 mm was 0.35%.

I should like to thank Academicians N. N. Bogolyubov and A. M. Baldin and Professor N. E. Tyurin for supporting this work, É. I. Denisov, V. I. Glebov, M. A. Kumakhov, V. A. Bazylev and V. I. Tumanov for assistance in the work and discussions and also the collectives at the Laboratory of High Energies at the Joint Institute for Nuclear Research and the personnel of the accelerator of the Institute of High Energy Physics at Serpukhov for assistance in these investigations.

[1]M. A. Kumakhov, Phys. Lett. **57 A**, 17 (1976).
[2]I. I. Miroshnichenko *et al.*, Pis'ma Zh. Eksp. Teor. Fiz. **29**, 786 (1979) [JETP Lett. **29**, 722 (1979)]; R. O. Avakyan *et al.*, Zh. Eksp. Teor. Fiz. **82**, 1825 (1982) [Sov. Phys. JETP **55**, 1052 (1982)].
[3]V. M. Golovatyuk, I. M. Ivanchenko, R. B. Kadyrov *et al.*, Preprint D1-81-592 [in Russian], JINR, Dubna (1981); FERMILAB Pub-81/34-Exp, Batavia (1981); Phys. Rev. Lett. **48**, 488 (1982); Nucl. Instrum. Methods **194**, 239 (1982).
[4]N. K. Bulgakov, A. S. Vodop'yanov, I. Voĭtkovska *et al.*, Preprint 1-83-731 [in Russian], JINR, Dubna (1983).
[5]N. K. Bulgakov, A. S. Vodop'yanov, I. Voĭtkovska *et al.*, Preprint 1-83-603 [in Russian], JINR, Dubna (1983); Pis'ma Zh. Eksp. Teor. Fiz. **38**, 462 (1983) JETP Lett. **38**, 561 (1983)].
[6]N. K. Buigakov, A. S. Vodop'yanov, I. Voĭtkovska *et al.*, Preprint 1-83-621 [in Russian], JINR, Dubna (1983).
[7]N. K. Bulgakov, A. S. Vodop'yanov, V. M. Golovatyuk *et al.*, Preprint 1-83-640 [in Russian], JINR, Dubna (1983).
[8]N. K. Bulgakov, A. S. Vodop'yanov, I. Voĭtkovska *et al.*, Preprint R1-85-27 [in Russian], JINR, Dubna (1985).
[9]N. K. Bulgakov, A. S. Vodop'yanov, I. Voĭtkovska *et al.*, Preprint Rl-85-28 [in Russian], JINR, Dubna (1985).
[10]N. K. Bulgakov, A. S. Vodop'yanov, I. Voĭtkovska *et al.*, Zh. Eksp. Teor. Fiz. **90**, 1527 (1986) Sov. Phys. JETP **63**, 898 (1986)].
[11]N. K. Bulgakov, A. S. Vodop'yanov, I. Voĭtkovska *et al.*, Preprint 1-84-630 [in Russian], JINR, Dubna (1984).
[12]N. K. Bulgakov, A. S. Vodop'yanov, I. Voĭtkovska *et al.*, Preprint 1-84-639 [in Russian], JINR, Dubna (1984).
[13]N. K. Bulgakov, A. S. Vodop'yanov, I. Voĭtkovska *et al.*, Preprint 1-84-372 [in Russian], JINR, Dubna (1984).
[14]N. K. Bulgakov, A. S. Vodop'yanov, I. Voĭtkovska *et al.*, Preprint R1-85-670 [in Russian], JINR, Dubna (1985).
[15]N. K. Bulgakov, A. S. Vodop'yanov, I. Voĭtkovska *et al.*, Preprint R1-85-671 [in Russian], JINR, Dubna (1985).
[16]N. K. Bulgakov, A. S. Vodop'yanov, I. Voĭtkovska *et al.*, Preprint R1-85-672 [in Russian], JINR, Dubna (1985).
[17]A. S. Vodop'yanov, I. Voĭtpovska, and V. M. Golovatyuk *et al.*, Preprint R13-82-547 [in Russian], JINR, Dubna (1982); Nucl. Instrum. Methods **211**, 353 (1983).
[18]M. D. Bavizhev, N. K. Bulgakov, A. S. Vodop'yanov *et al.*, Preprint R13-81-644 in [Russian], JINR, Dubna (1981); Nucl. Instrum. Methods **206**, 379 (1983).
[19]I. Voĭtkovska, V. M. Golovatyuk, Z. Guzik *et al.*, Preprint R13-82-374 [in Russian], JINR, Dubna (1982); Nucl. Instrum. Methods **215**, 135 (1983).
[20]M. D. Bavizhev, N. K. Bulgakov, I. Voĭtkovska *et al.*, Preprint 82-74 OP [in Russian], Institute of High Energy Physics, Serpukhov (1982).
[21]N. K. Bulgakov. I. Voĭtkovska, V. M. Golovatyuk *et al.*, Prib. Tekh. Eksp. **4**, 53 (1986).
[22]N. K. Bulgakov, I. Voĭtkovska, V. M. Golovatyuk *et al.*, Preprint 13-84-676 [in Russian], JINR, Dubna (1986).
[23]A. I. Akhiezer *et al.*, Preprint 77-38 [in Russian], Physicotechnical Institute, Kharkov (1977); V. N. Baĭer *et al.*, Preprint 81-139 [in Russian], Institute of Nuclear Physics, Novosibirsk (1981); V. N. Baier *et al.*, Phys. Lett. **73A**, 414 (1979); V. A. Bazylev *et al.*, Zh. Eksp. Teor. Fiz. **80**, 608 (1981) Sov. Phys. JETP **53**, 306 (1981)]; V. N. Baier *et al.*, Preprint 84-116 [in Russian], Institute of Nuclear Physics, Novosibirsk (1984); M. Kh. Khokonov, Radiat. Eff. **80**, 93 (1984); N. I. Zimin, Preprint 1-83-729 [in Russian], JINR, Dubna (1983); N. F. Shul'ga *et al.*, Zh. Eksp. Teor. Fiz. **87**, 250 (1984) [Sov. Phys. JETP **60**, 145 (1984)]; A. I. Akhiezer *et al.*, Usp. Fiz. Nauk **137**, 561 (1982) Sov. Phys. Usp. **25**, 541 (1982)]; N. I. Zimin, Preprint R1-83-294 [in Russian], JINR, Dubna (1983).

Translated by Julian B. Barbour